

Entanglement Asymmetry and Quantum Mpemba Effect for Non-Abelian Global Symmetry

Harunobu Fujimura and Soichiro Shimamori

*Department of Physics, The University of Osaka, Machikaneyama-Cho 1-1, Toyonaka 560-0043,
Japan*

September 2025

Abstract

Entanglement asymmetry is a measure that quantifies the degree of symmetry breaking at the level of a subsystem. In this work, we investigate the entanglement asymmetry in $\widehat{su}(N)_k$ Wess-Zumino-Witten model and discuss the quantum Mpemba effect for $SU(N)$ symmetry, the phenomenon that the more symmetry is initially broken, the faster it is restored. Due to the Coleman–Mermin–Wagner theorem, spontaneous breaking of continuous global symmetries is forbidden in $1+1$ dimensions. To circumvent this no-go theorem, we consider excited initial states which explicitly break non-Abelian global symmetry. We particularly focus on the initial states built from primary operators in the fundamental and adjoint representations. In both cases, we study the real-time dynamics of the Rényi entanglement asymmetry and provide clear evidence of quantum Mpemba effect for $SU(N)$ symmetry. Furthermore, we find a new type of quantum Mpemba effect for the primary operator in the fundamental representation: increasing the rank N leads to stronger initial symmetry breaking but faster symmetry restoration. Also, increasing the level k leads to weaker initial symmetry breaking but slower symmetry restoration. On the other hand, no such behavior is observed for adjoint case, which may suggest that this new type of quantum Mpemba effect is not universal.

Contents

1	Introduction	1
2	Entanglement asymmetry in quantum field theories	3
2.1	Symmetry operators	3
2.2	Entanglement asymmetry	4
2.3	Replica trick and operator insertion	7
2.4	Entanglement asymmetry in $(1 + 1)$ -dimensional CFT	9
3	Quantum Mpemba effect: fundamental case	11
3.1	Exact results	12
3.2	Asymptotic behaviors	13
3.3	Quantum Mpemba effect for $SU(N)$ symmetry	16
3.4	New type of quantum Mpemba effect	18
4	Quantum Mpemba effect: adjoint case	22
5	Conclusion and discussion	26
A	Four-point function in Wess-Zumino-Witten models	27
A.1	Preliminary	27
A.2	Knizhnik-Zamolodchikov equation	28
A.3	Computing the four-point function for $\widehat{su}(N)_k$	29
B	Asymptotic behavior of EA_2 in $\widehat{su}(N)_k$ WZW model	33

1 Introduction

Symmetry breaking is one of the most fundamental concepts in modern physics, ranging from high energy physics to condensed matter physics. Traditionally, the symmetry breaking is characterized through order parameters such as magnetization and chiral condensation. However, formulating the symmetry breaking in non-equilibrium systems is much more subtle, and it is necessary to introduce more suitable quantity to capture and quantify it.

As one way to characterize the symmetry breaking for non-equilibrium systems, *entanglement asymmetry* was proposed in [1] as a measure to quantify the degree of symmetry breaking at the level of subsystem. Let G be the symmetry of interest and ρ_A the reduced density matrix of a subsystem A . As reviewed in the main text, one can define the symmetrized reduced density matrix, denoted by $\rho_{A,G}$, obtained by projecting ρ_A onto the G -invariant subspace. The entanglement asymmetry is then defined as the relative entropy between ρ_A and $\rho_{A,G}$:

$$\Delta S_A = \text{Tr}_A [\rho_A (\log \rho_A - \log \rho_{A,G})]. \quad (1.1)$$

By construction, the entanglement asymmetry is non-negative and vanishes if and only if the subsystem A preserves the symmetry G [2]. The entanglement asymmetry has been studied in various contexts e.g., [3–8].

One of the most mysterious phenomena in non-equilibrium systems is the *quantum Mpemba effect* through symmetry restoration. This is a phenomenon that the more symmetry is initially broken, the faster it is restored. While originally studied from a purely theoretical perspective, the quantum Mpemba effect has recently been experimentally observed in trapped-ion quantum simulators [9–12]. In recent studies, it has been revealed that the entanglement asymmetry can be used to describe this counterintuitive phenomenon in various quantum systems, e.g., one-dimensional spin chains [13–22], two-dimensional spin systems [23, 24], and conformal field theories (CFTs) [25].¹ For more detail, we refer the readers to recent reviews [35, 36].

While the studies mentioned in the previous paragraph focus mainly on the restoration of Abelian symmetries including $U(1)$ or \mathbb{Z}_N , the quantum Mpemba effect for non-Abelian symmetries remains essentially elusive.² In this work, we present the detailed analysis on the symmetry restoration structures for non-Abelian symmetries by using the $\widehat{su}(N)_k$ Wess-Zumino-Witten (WZW) models through the lens of entanglement asymmetry. Due to the Coleman–Mermin–Wagner theorem [38, 39], spontaneous breaking of continuous global symmetries in $1 + 1$ dimensions is forbidden. To bypass this no-go theorem, we consider an excited initial state $|\mathcal{O}\rangle = \mathcal{O}|0\rangle$, created by a local primary operator \mathcal{O} carrying non-trivial charges under the non-Abelian symmetry [40]. For concreteness, we focus on WZW primaries in the fundamental and adjoint representations.

Given the difficulty of computing entanglement asymmetry directly, we instead evaluate the n -th Rényi entanglement asymmetry $\Delta S_A^{(n)}$ which yields the entanglement asymmetry in the limit $n \rightarrow 1$. Crucially, conformal symmetry enables us to express these Rényi entanglement asymmetries in terms of $2n$ -point correlation functions, which are tractable via CFT techniques. In particular, we compute the second Rényi entanglement asymmetry (i.e., $n = 2$) using exact four-point functions, which are obtained analytically by solving the Knizhnik–Zamolodchikov equations [41] and are explicitly known in [42, 43].

With these exact results, we analyze the Rényi entanglement asymmetry in WZW model and explore various asymptotic regimes, such as the long-time limit and the large-interval limit. We also investigate the real-time dynamics of the Rényi entanglement asymmetry and provide clear evidence of the quantum Mpemba effect for $SU(N)$ symmetry in both cases of fundamental and adjoint primaries. More interestingly, for the initial state built from the primary in the fundamental representation, we uncover a new type of quantum Mpemba effect: increasing the rank N amplifies the initial symmetry breaking, while accelerating

¹In the context of quantum information theory, the quantum Mpemba effect has also been investigated in random quantum circuits [26–32] and in periodically driven quantum systems [33, 34].

²Although the entanglement asymmetries for non-Abelian symmetries are discussed in [6–8, 37], the quantum Mpemba effects are not discussed. Also, while the quantum Mpemba effects for non-Abelian global symmetries are discussed for random states [26, 31], the continuum examples have not been explored so far.

the symmetry restoration. Conversely, increasing the level k weakens the initial symmetry breaking, while decelerating the symmetry restoration. Such a realization of quantum Mpemba effect though symmetry restoration has not been reported in previous works. On the other hand, in the case of adjoint primary, we are not able to find any evidence for this new type of quantum Mpemba effect. This may suggest that this quantum Mpemba effect is not a universal phenomenon although we have not explored other representations. We leave further analysis about this new type of quantum Mpemba effect to future studies.

This paper is organized as follows. In Section 2, we review the definition and basic properties of the entanglement asymmetry in quantum field theories and explain how it can be expressed in terms of correlation functions. In Section 3, we derive the exact result of second Rényi entanglement asymmetry for the initial state build from the fundamental primary, and analyze its asymptotic behavior as well as the quantum Mpemba effect. In Section 4, we analyze the symmetry restoration structures for the initial state constructed from the WZW current in the adjoint representation. Finally, in Section 5, we summarize this paper and list some future directions. In Appendix A, we review the four-point function of two fundamental and two anti-fundamental primaries. In Appendix B, we give detailed analysis on asymptotic behaviors of the second Rényi entanglement asymmetry.

2 Entanglement asymmetry in quantum field theories

In this section, we provide a brief review of entanglement asymmetry and Rényi entanglement asymmetry introduced in [1] and discuss how to analyze the Rényi entanglement asymmetry in conformal field theories (CFTs). From the perspective of the replica trick [44–46] and the symmetry operators [47], the Rényi entanglement asymmetry can be expressed in terms of correlation functions.

2.1 Symmetry operators

Before introducing the entanglement asymmetry, we briefly review the symmetry operators [47], which will be necessary later. For a more comprehensive introduction to symmetry operators, we refer the readers to the recent review on generalized symmetries [48]. For simplicity, let us consider quantum field theories with group-like global symmetry G on the two-dimensional Euclidean spacetime. Every group element $g \in G$ is associated to the corresponding symmetry operator $U_\Sigma(g)$, where Σ is one-dimensional manifold in two-dimensional spacetime. The symmetry operator $U_\Sigma(g)$ is topological in a sense that the correlation function with $U_\Sigma(g)$ inserted is invariant under continuous and smooth deformation of $\Sigma \rightarrow \Sigma'$. This topological property can be rephrased by the following operator equation:

$$U_\Sigma(g) = U_{\Sigma'}(g) . \quad (2.1)$$

Moreover, this symmetry operator inherits the group structure of G , namely,

$$U_\Sigma(g_1)U_\Sigma(g_2) = U_\Sigma(g_1g_2) , \quad \forall g_1, g_2 \in G . \quad (2.2)$$

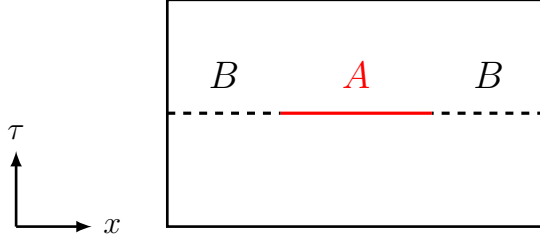


Figure 1: The sketch of subregions A and B in two-dimensional Euclidean spacetime. Here subregion B is defined as the total system excluding the subregion A .

which is schematically expressed as

$$(2.3)$$

where the blue line labeled by g represents the symmetry operator $U_\Sigma(g)$, and the box means the entire spacetime. The transformation of an operator $\mathcal{O}(x)$ under a group element $g \in G$ is described by the symmetry operator as

$$U_\Sigma^\dagger(g)\mathcal{O}(x)U_\Sigma(g) = R(g)\mathcal{O}(x) , \quad x \in \Sigma , \quad (2.4)$$

where $R(g)$ denotes a representation of g of \mathcal{O} . Diagrammatically, this rule is depicted as follows:

$$(2.5)$$

2.2 Entanglement asymmetry

In this subsection, we introduce the concept of entanglement asymmetry [1]. We divide the total spacial region into two subregions A and B , as illustrated in Fig. 1. We assume that the total Hilbert space \mathcal{H}_{tot} decomposes into a tensor product as

$$\mathcal{H}_{\text{tot}} = \mathcal{H}_A \otimes \mathcal{H}_B , \quad (2.6)$$

where $\mathcal{H}_{A/B}$ denote the Hilbert spaces of subsystems A/B , respectively. With this decomposition, the symmetry operator $U_\Sigma(g)$ factorizes as

$$U_\Sigma(g) = U_A(g) \otimes U_B(g) , \quad (2.7)$$

where Σ is chosen to be the spatial slice at fixed time, $\Sigma = A \cup B$, and $U_{A/B}(g)$ denote the symmetry operators acting on the Hilbert spaces $\mathcal{H}_{A/B}$, respectively. The reduced density matrix ρ_A of the subsystem A is defined by tracing out the degrees of freedom on subsystem B from the total density matrix ρ_{tot} :

$$\rho_A \equiv \text{Tr}_B [\rho_{\text{tot}}] . \quad (2.8)$$

Under the action of a group element g , the reduced density matrix ρ_A transforms as $\rho_A \mapsto U_A(g)\rho_A U_A^\dagger(g)$. This means that when the global symmetry G is preserved in the subsystem A , the reduced density matrix has to commute with the symmetry operator $U_\Sigma(g)$ for $\forall g \in G$:

$$[\rho_A, U_A(g)] = 0 \quad (\text{symmetry preserved}) . \quad (2.9)$$

Otherwise, the symmetry G is said to be broken in the subsystem A :

$$[\rho_A, U_A(g)] \neq 0 \quad (\text{symmetry broken}) . \quad (2.10)$$

To define the entanglement asymmetry, we introduce the symmetrized reduced density matrix [4]:

$$\rho_{A,G} \equiv \int_G dg \, U_A(g) \rho_A U_A^\dagger(g) , \quad (2.11)$$

where dg denotes the Haar measure on the group G , normalized as $\int_G dg = 1$ ³. By construction, the symmetrized reduced density matrix $\rho_{A,G}$ always commutes with the symmetry operator $U_A(g)$. With this definition, the criterion for symmetry preservation/breaking in A described above can be expressed as

$$\begin{cases} \rho_A = \rho_{A,G} & (\text{Symmetry preserved}) \\ \rho_A \neq \rho_{A,G} & (\text{Symmetry broken}) \end{cases} \quad (2.12)$$

In quantum information theory, the distinguishability between two density matrices ρ and σ can be quantified by relative entropy [49]. The entanglement asymmetry is thus naturally defined as the relative entropy between ρ_A and $\rho_{A,G}$:

$$\Delta S_A \equiv \text{Tr}_A [\rho_A (\log \rho_A - \log \rho_{A,G})] . \quad (2.13)$$

Importantly, the entanglement asymmetry satisfies the following property [2, 49]:

$$\begin{cases} \Delta S_A = 0 & \iff \rho_A = \rho_{A,G} \\ \Delta S_A > 0 & \iff \rho_A \neq \rho_{A,G} \end{cases} . \quad (2.14)$$

³For a discrete group, the symmetrized reduced density matrix can be defined in the same way, with replacement $\int_G dg \rightarrow \frac{1}{|G|} \sum_{g \in G}$.

By combining this with (2.12), we can regard the entanglement asymmetry as a quantitative measure of symmetry breaking at the level of the subsystem A . In general, analyzing the entanglement asymmetry is challenging due to the presence of $\log \rho$ in its definition. It is therefore convenient to introduce the Rényi entanglement asymmetry:

$$\Delta S_A^{(n)} \equiv \frac{1}{1-n} (\log \text{Tr}_A [\rho_{A,G}^n] - \log \text{Tr}_A [\rho_A^n]) , \quad (2.15)$$

where n is a positive integer. The entanglement asymmetry in (2.13) is recovered by analytic continuation of the Rényi entanglement asymmetry and taking the following limit:

$$\lim_{n \rightarrow 1} \Delta S_A^{(n)} = \Delta S_A . \quad (2.16)$$

Let us rewrite the Rényi entanglement asymmetry in terms of the symmetry operators. Substituting the definition of the symmetrized reduced density matrix in (2.11) into $\text{Tr}_A [\rho_{A,G}^n]$, we obtain the following:

$$\begin{aligned} \text{Tr}_A [\rho_{A,G}^n] &= \int_G dh_1 \cdots dh_n \text{Tr}_A \left[U_A(h_1) \rho_A U_A^\dagger(h_1) \cdot U_A(h_2) \rho_A U_A^\dagger(h_2) \cdots U_A(h_n) \rho_A U_A^\dagger(h_n) \right] \\ &= \int_G dh_1 \cdots dh_n \text{Tr}_A \left[\rho_A U_A(h_1^{-1} h_2) \rho_A U_A(h_2^{-1} h_3) \cdots \rho_A U_A(h_n^{-1} h_1) \right] , \end{aligned} \quad (2.17)$$

where we used the cyclic property of trace and the fusion rule (2.2). By changing integral variables as $g_i^{-1} = h_i^{-1} h_{i+1}$ for $i = 1, \dots, n$, ($h_{n+1} \equiv h_1$), we arrive at⁴

$$\text{Tr}_A [\rho_{A,G}^n] = \int_G dg_1 \cdots dg_{n-1} \text{Tr}_A \left[\rho_A U_A(g_1^{-1}) \cdots \rho_A U_A(g_{n-1}^{-1}) \cdot \rho_A U_A(g_{n-1} \cdots g_1) \right] . \quad (2.18)$$

We now define the charged moments $Z(g_1, \dots, g_{n-1})$ as

$$Z(g_1, \dots, g_{n-1}) \equiv \frac{\text{Tr}_A [\rho_A U_A(g_1^{-1}) \cdots \rho_A U_A(g_{n-1}^{-1}) \cdot \rho_A U_A(g_{n-1} \cdots g_1)]}{\text{Tr}_A [\rho_A^n]} . \quad (2.19)$$

In terms of the charged moment, the Rényi entanglement asymmetry can be expressed as

$$\Delta S_A^{(n)} = \frac{1}{1-n} \log \left[\int_G dg_1 \cdots dg_{n-1} Z(g_1, \dots, g_{n-1}) \right] . \quad (2.20)$$

To evaluate the charged moments $Z(g_1, \dots, g_{n-1})$, we employ the path integral formulation, as explained in the next subsection.

⁴Note that the g_n does not appear in the integrand, and its integration simply yields $\int_G dg_n = 1$.

2.3 Replica trick and operator insertion

Let us now consider the path integral representation of the charged moments. In the case where the quantum state of the total system is vacuum, i.e., $\rho_{\text{tot}} = |0\rangle\langle 0|$, the quantity $\text{Tr}_A[\rho_A^n]$ is given by the partition function on the n -sheeted manifold \mathcal{R}_n [45, 46]. In this case, a charged moment is identified with the partition function on the n -sheeted manifold \mathcal{R}_n with the insertion of symmetry operators [50, 51].

To investigate the dynamics of symmetry restoration, we have to consider an initially symmetry breaking state. However, in $1+1$ dimensions, the Coleman-Mermin-Wagner theorem [38, 39] forbids *spontaneous* breaking of continuous symmetries. Therefore, we focus on an initial quantum state which *explicitly* breaks the global symmetry G . As such a state, we prepare an initial state $|\psi\rangle$ by inserting a local operator \mathcal{O} [40, 52]:

$$|\psi\rangle = \frac{1}{\sqrt{Z_{\mathcal{O}}}} \mathcal{O}(z_-, \bar{z}_-) |0\rangle, \quad (2.21)$$

where $Z_{\mathcal{O}}$ is the normalization constant fixed by $\langle\psi|\psi\rangle = 1$ and $z_- = x_0 - i\tau_0$ denotes the insertion point in complex coordinates. The real-time evolution of the density matrix is obtained by analytical continuation from Euclidean time [40, 52]:

$$\begin{aligned} \rho_{\text{tot}}(t) &= e^{-iHt} |\psi\rangle \langle\psi| e^{iHt} \\ &= \frac{1}{Z_{\mathcal{O}}} \mathcal{O}(z_-(t), \bar{z}_-(t)) |0\rangle \langle 0| \mathcal{O}^\dagger(z_+(t), \bar{z}_+(t)), \end{aligned} \quad (2.22)$$

where $z_{\pm}(t) = x_0 \pm i\tau_0 + t$, $\bar{z}_{\pm}(t) = x_0 \mp i\tau_0 - t$.⁵ The reduced density matrix $\rho_A = \text{Tr}_B[|\psi\rangle\langle\psi|]$ can then be represented as a path integral form:

$$\rho_A = \frac{1}{Z_{\mathcal{O}}} \left[\begin{array}{c} \mathcal{O}^\dagger \\ \times \\ \times \\ \mathcal{O} \end{array} \right] \begin{array}{c} \text{---} \\ \text{---} \end{array} \begin{array}{l} \tau = +0 \\ \tau = -0 \end{array}. \quad (2.23)$$

From this representation, the trace $\text{Tr}_A[\rho_A^n]$ can be expressed as a path integral over the

⁵In our notation, \bar{z} is not complex conjugate to z in Minkowski spacetime.

n -sheeted manifold \mathcal{R}_n [45, 46].

$$\text{Tr}_A [\rho_A^n] = \frac{1}{Z_{\mathcal{O}}^n} \times \left(\text{Diagram of } n \text{ sheets with operator insertions} \right) = \frac{1}{Z_{\mathcal{O}}^n Z_n} \left\langle \prod_{i=1}^n \mathcal{O}_i \mathcal{O}_i^\dagger \right\rangle_{\mathcal{R}_n}, \quad (2.24)$$

where $\mathcal{O}_i = \mathcal{O}(z_{i,-}, \bar{z}_{i,-})$, $\mathcal{O}_i^\dagger = \mathcal{O}^\dagger(z_{i,+}, \bar{z}_{i,+})$ and $z_{i,\pm}$ denote the operator insertion points on the i -th sheet. The constant Z_n denotes the partition function of n -sheeted manifold \mathcal{R}_n . The numerator in charged moments (2.19) can be evaluated in a similar way.

$$(\text{Numerator in (2.19)}) = \frac{1}{Z_{\mathcal{O}}^n} \times \left(\text{Diagram of n sheets with symmetry operators} \right)$$

To simplify this expression, we make use of the topological property of symmetry operators⁶ As depicted in Fig. 2, we can move the symmetry operator on the i -th sheet to the $(i+1)$ -th sheet ($i = 1, \dots, n-1$) [25]. During this deformation, the symmetry operator acts on the operators \mathcal{O}_i and \mathcal{O}_i^\dagger , which transform as (2.4). By repeating these deformations $(n-1)$

⁶One might concern about the presence of the boundary of subregion A [53]. Here we consider the symmetric boundary condition at the edge of entangling surface ∂A and the symmetry operators are also topological there. This means that the inserted local operators are only sources for symmetry breaking.

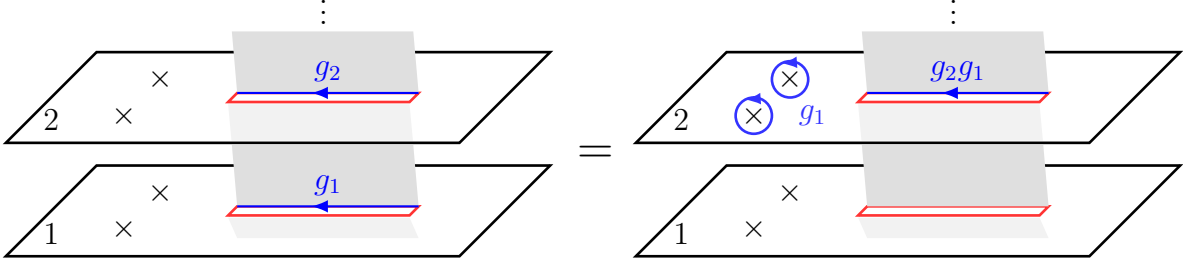


Figure 2: The symmetry operators on an n -sheeted manifold can be topologically deformed. For example, the symmetry operator $U_A(g_1)$ on the first sheet can be moved to the second sheet and fuse with the symmetry operator $U_A(g_2)$ there. As a result, the operators on the second sheet transform as $\mathcal{O}_2 \rightarrow U_\Sigma^\dagger(g_1)\mathcal{O}_2 U_\Sigma(g_1)$. The same applies to the remaining sheets.

times, we arrive at the following expressions:

$$\begin{aligned}
 (\text{Numerator in (2.19)}) &= \frac{1}{Z_{\mathcal{O}}^n} \times \\
 &\quad \text{[Diagram showing sheets 1, 2, ..., n with operators g1, g2, ..., gn-1 fused on sheet n]} \\
 &= \frac{1}{Z_{\mathcal{O}}^n Z_n} \left\langle \mathcal{O}_1 \mathcal{O}_1^\dagger \prod_{i=2}^n [R(g_{i-1} \cdots g_1) \mathcal{O}_i] [\bar{R}(g_{i-1} \cdots g_1) \mathcal{O}_i^\dagger] \right\rangle_{\mathcal{R}_n}. \quad (2.25)
 \end{aligned}$$

Substituting (2.24) and (2.25) into (2.19), the charged moment can be expressed in terms of correlation functions

$$Z(g_1, \cdots, g_{n-1}) = \frac{\left\langle \mathcal{O}_1 \mathcal{O}_1^\dagger \prod_{i=2}^n [R(g_{i-1} \cdots g_1) \mathcal{O}_i] [\bar{R}(g_{i-1} \cdots g_1) \mathcal{O}_i^\dagger] \right\rangle_{\mathcal{R}_n}}{\left\langle \prod_{i=1}^n \mathcal{O}_i \mathcal{O}_i^\dagger \right\rangle_{\mathcal{R}_n}}. \quad (2.26)$$

2.4 Entanglement asymmetry in $(1+1)$ -dimensional CFT

In the case of a $(1+1)$ -dimensional CFT, the charged moments (2.26) can be further simplified. The n -sheeted manifold \mathcal{R}_n can be mapped to plane via the following conformal

transformation [25, 52, 54]:

$$z \rightarrow \zeta = \left(\frac{z}{z - \ell} \right)^{1/n}, \quad (2.27)$$

where we take the interval as $A = [0, \ell]$. Under this mapping, the correlation functions appearing in the charged moments reduce to those on the plane:

$$Z(g_1, \dots, g_{n-1}) = \frac{\left\langle \tilde{\mathcal{O}}_1 \tilde{\mathcal{O}}_1^\dagger \prod_{i=2}^n \left[R(g_{i-1} \dots g_1) \tilde{\mathcal{O}}_i \right] \left[\bar{R}(g_{i-1} \dots g_1) \tilde{\mathcal{O}}_i^\dagger \right] \right\rangle_{\text{Plane}}}{\left\langle \prod_{i=1}^n \tilde{\mathcal{O}}_i \tilde{\mathcal{O}}_i^\dagger \right\rangle_{\text{Plane}}}, \quad (2.28)$$

where $\tilde{\mathcal{O}}_i = \mathcal{O}(\zeta_{1,-}, \bar{\zeta}_{1,-})$, and $\tilde{\mathcal{O}}_i^\dagger = \mathcal{O}^\dagger(\zeta_{1,+}, \bar{\zeta}_{1,+})$. The conformal factors cancel in the numerator and the denominator in the charged moments. The coordinates $\zeta_{i,\pm}$ on the plane are given by

$$\zeta_{i,\pm}(t) = \left(\frac{z_\pm(t)}{z_\pm(t) - \ell} \right)^{1/n} \exp \left(\frac{2\pi i}{n} (i-1) \right), \quad i = 1, \dots, n. \quad (2.29)$$

In the following, we focus on the second Rényi entanglement asymmetry (EA₂) by restricting to $n = 2$. In this case, the charged moments reduce to the ratio of four-point functions:

$$Z(g) = \frac{\left\langle \tilde{\mathcal{O}}_1 \tilde{\mathcal{O}}_1^\dagger \left[R(g) \tilde{\mathcal{O}}_2 \right] \left[\bar{R}(g) \tilde{\mathcal{O}}_2^\dagger \right] \right\rangle_{\text{Plane}}}{\left\langle \tilde{\mathcal{O}}_1 \tilde{\mathcal{O}}_1^\dagger \tilde{\mathcal{O}}_2 \tilde{\mathcal{O}}_2^\dagger \right\rangle_{\text{Plane}}}, \quad (2.30)$$

with the coordinates $\zeta_{i,\pm}(t)$:⁷

$$\zeta_{1,\pm}(t) = -\zeta_{2,\pm}(t) = \sqrt{\frac{x_0 + t \pm i\tau_0}{x_0 + t - \ell \pm i\tau_0}}, \quad \bar{\zeta}_{1,\pm}(t) = -\bar{\zeta}_{2,\pm}(t) = \sqrt{\frac{x_0 - t \mp i\tau_0}{x_0 - t - \ell \mp i\tau_0}}, \quad (2.31)$$

where we define the square root of complex function as

$$\sqrt{\omega} = \sqrt{r} e^{i\theta/2}, \quad \theta \in [-\pi, \pi), \quad \omega = \frac{z}{z - \ell}. \quad (2.32)$$

Here, we choose the branch cut along the negative real axis in the ω -plane, which corresponds to $A = [0, \ell]$ in the original z -plane.

We further perform the following conformal transformation:

$$\xi = \frac{(\zeta - \zeta_{2,+})(\zeta_{1,+} - \zeta_{2,-})}{(\zeta - \zeta_{2,-})(\zeta_{1,+} - \zeta_{2,+})}. \quad (2.33)$$

⁷Here we follow the convention used in [52]

This conformal transformation maps the coordinates $(\zeta_{1,-}, \zeta_{1,+}, \zeta_{2,-}, \zeta_{2,+}) \mapsto (x, 1, \infty, 0)$ and the cross-ratios x and \bar{x} is given by⁸

$$x(t) = \begin{cases} \frac{1}{2} + \frac{1}{2} \left[1 + \left(\frac{\tau_0 \ell}{(t+x_0)(t+x_0-\ell) + \tau_0^2} \right)^2 \right]^{-1/2} & \text{for } (t+x_0)(t+x_0-\ell) + \tau_0^2 \geq 0 \\ \frac{1}{2} - \frac{1}{2} \left[1 + \left(\frac{\tau_0 \ell}{(t+x_0)(t+x_0-\ell) + \tau_0^2} \right)^2 \right]^{-1/2} & \text{for } (t+x_0)(t+x_0-\ell) + \tau_0^2 < 0 \end{cases}, \quad (2.34)$$

$$\bar{x}(t) = \begin{cases} \frac{1}{2} + \frac{1}{2} \left[1 + \left(\frac{\tau_0 \ell}{(t-x_0)(t-x_0+\ell) + \tau_0^2} \right)^2 \right]^{-1/2} & \text{for } (t-x_0)(t-x_0+\ell) + \tau_0^2 \geq 0 \\ \frac{1}{2} - \frac{1}{2} \left[1 + \left(\frac{\tau_0 \ell}{(t-x_0)(t-x_0+\ell) + \tau_0^2} \right)^2 \right]^{-1/2} & \text{for } (t-x_0)(t-x_0+\ell) + \tau_0^2 < 0 \end{cases}, \quad (2.35)$$

It turns out that the conformal factors are again canceled in the numerator and the denominator in (2.30), then the EA₂ reduces to

$$\Delta S_A^{(2)}(t) = -\log \left[\int_G dg \frac{\langle \mathcal{O}(x(t), \bar{x}(t)) \mathcal{O}^\dagger(1, 1) [R(g)\mathcal{O}](\infty, \infty) [\bar{R}(g)\mathcal{O}^\dagger](0, 0) \rangle}{\langle \mathcal{O}(x(t), \bar{x}(t)) \mathcal{O}^\dagger(1, 1) \mathcal{O}(\infty, \infty) \mathcal{O}^\dagger(0, 0) \rangle} \right]. \quad (2.36)$$

Here, we omitted the subscript “Plane” in the correlation functions, and all operators in this expression are defined on the plane. From this expression, the EA₂ is determined by four-point functions, which are well studied in the context of CFTs.

3 Quantum Mpemba effect: fundamental case

In previous section, we expressed EA₂ in terms of the four-point conformal correlators. The main goal of this section is to explore the symmetry restoration structure in $\widehat{su}(N)_k$ WZW model by focusing on the initial state built from primary operator $\Phi_i(z, \bar{z}) = \Phi_i(z) \otimes \bar{\Phi}_i(\bar{z})$ in the fundamental representation.⁹ (The index i runs from 1 to N .)

⁸See also footnote 5.

⁹In principle, one can consider the most general state as $\Phi_{ij}(z, \bar{z}) = \Phi_i(z) \otimes \bar{\Phi}_j(\bar{z})$. In this paper, for simplicity, we restrict to the diagonal case: $i = j$.

3.1 Exact results

In this case, EA_2 can be written in the following decomposed form:¹⁰

$$\Delta S_A^{(2)}(t) = -\log \left[\frac{\sum_{j,k} \sum_{j',k'} \sum_{A,B=1}^2 (M_4)^{jj'ii}_{iikk'} (I_A)^{ki}_{ij} (\bar{I}_B)^{k'i}_{ij'} G_{A,B}(t)}{\sum_{A,B=1}^2 G_{A,B}(t)} \right], \quad (3.1)$$

where M is given by the integral [55]

$$\begin{aligned} M_{iikk'}^{jj'ii} &= \int_{\text{SU}(N)} dg [R(g)]_i^j [R(g)]_i^{j'} [R^{-1}(g)]_k^i [R^{-1}(g)]_{k'}^i \\ &= \frac{1}{N(N+1)} \left(\delta_k^j \delta_{k'}^{j'} + \delta_{k'}^j \delta_k^{j'} \right), \end{aligned} \quad (3.2)$$

and I_A and \bar{I}_B are invariant tensors in $\mathbf{N} \otimes \bar{\mathbf{N}} \otimes \bar{\mathbf{N}} \otimes \mathbf{N}$ for holomorphic and anti-holomorphic sectors, respectively. Also, $G_{A,B}(t) \equiv G_{A,B}(x(t), \bar{x}(t))$ is the four-point function associated to the invariant tensors I_A and \bar{I}_B , which can be derived by solving the Knizhnik-Zamolodchikov equation [41]:

$$G_{AB}(t) = f(t) \left[F_A^{(-)}(x(t)) F_B^{(-)}(\bar{x}(t)) + \frac{1 - c_{--}^2}{c_{+-}^2} F_A^{(+)}(x(t)) F_B^{(+)}(\bar{x}(t)) \right], \quad (3.3)$$

where $f(t)$ is the function which does not depend on the indices A and B . Also, c_{--} and c_{+-} are constants given by

$$c_{--} = N \frac{\Gamma(\frac{N}{N+k}) \Gamma(-\frac{N}{N+k})}{\Gamma(\frac{1}{N+k}) \Gamma(-\frac{1}{N+k})}, \quad c_{+-} = -N \frac{\Gamma(\frac{N}{N+k})^2}{\Gamma(\frac{N+1}{N+k}) \Gamma(\frac{N-1}{N+k})}, \quad (3.4)$$

and $F_A^{(\pm)}(x)$ are defined by

$$F_1^{(-)}(x) = F\left(\frac{1}{N+k}, -\frac{1}{N+k}; \frac{k}{N+k}; x\right), \quad (3.5)$$

$$F_1^{(+)}(x) = x^{\frac{N}{N+k}} F\left(\frac{N-1}{N+k}, \frac{N+1}{N+k}; 1 + \frac{N}{N+k}; x\right), \quad (3.6)$$

$$F_2^{(-)}(x) = \frac{1}{k} x F\left(1 + \frac{1}{N+k}, 1 - \frac{1}{N+k}; 2 - \frac{N}{N+k}; x\right), \quad (3.7)$$

$$F_2^{(+)}(x) = -N x^{\frac{N}{N+k}} F\left(\frac{N-1}{N+k}, \frac{N+1}{N+k}; \frac{N}{N+k}; x\right), \quad (3.8)$$

where $F(a, b; c; x)$ is the hypergeometric function. For completeness, we present the review on the four-point function in $\widehat{su}(N)_k$ WZW model in Appendix A. By plugging the above all results into (3.1), we can obtain the exact expression for EA_2 :

$$\Delta S_A^{(2)}(t) = -\log \left[\frac{2G_{1,1}(t) + (N+1)(G_{1,2}(t) + G_{2,1}(t)) + N(N+1)G_{2,2}(t)}{N(N+1) \sum_{A,B=1}^2 G_{A,B}(t)} \right]. \quad (3.9)$$

¹⁰Remark that, in this expression, the index i is fixed and we do not take the sum over i .

3.2 Asymptotic behaviors

In the previous subsection, we derived the exact result of EA_2 for an initial state build from the primary operator in the fundamental representation. However, due to the complexity of the expression, it is quite hard to give physical insights as it is. In this subsection, to get over this complexity, we investigate the behaviors of the exact result by taking various limits. We also give intrinsic interpretations of our results from the view point of the quasi-particle picture. For later convenience, we define dimensionless parameters $\tilde{\tau}_0$, \tilde{x}_0 , \tilde{t} as follows:

$$\tilde{\tau}_0 = \frac{\tau_0}{\ell}, \quad \tilde{x}_0 = \frac{x_0}{\ell}, \quad \tilde{t} = \frac{t}{\ell}. \quad (3.10)$$

Long time limit: $\tilde{t} \rightarrow \infty$.

In this limit, the asymptotic form of EA_2 (3.9) is given by

$$\Delta S_A^{(2)}(\tilde{t}) = \frac{(N-1)(N^2-2)}{N^2(N+1)} c_{N,k} \epsilon^{\frac{2N}{N+k}} + \frac{2}{k} \left(1 - \frac{1}{N}\right) \epsilon + \mathcal{O}\left(\epsilon^{1+\frac{2N}{N+k}}\right), \quad (3.11)$$

where the infinitesimally small parameter ϵ is given by

$$\epsilon = \frac{1}{4} \left(\frac{\tilde{\tau}_0}{\tilde{t}^2} \right)^2, \quad (3.12)$$

and the coefficient $c_{N,k}$ is defined as

$$c_{N,k} = \frac{\Gamma\left(\frac{k}{N+k}\right)^2 \Gamma\left(\frac{N-1}{N+k}\right) \Gamma\left(\frac{N+1}{N+k}\right)}{\Gamma\left(\frac{N}{N+k}\right)^2 \Gamma\left(\frac{k-1}{N+k}\right) \Gamma\left(\frac{k+1}{N+k}\right)} \geq 0. \quad (3.13)$$

The detailed derivation is provided in Appendix B. Note that EA_2 is always non-negative and EA_2 decays to zero as $\tilde{t} \rightarrow \infty$. This property is in line with our intuition since we start from a symmetry-breaking initial state and evolve it by the symmetry-preserving Hamiltonian. After sufficiently long time, the symmetry has to be restored in subsystem A , i.e., $\Delta S_A^{(2)}(\tilde{t} = \infty) = 0$.

Large interval limit: $\tilde{\tau}_0 \rightarrow 0$.

In this limit, the behavior of EA_2 depends on the sign of \tilde{x}_0 . For $\tilde{x}_0 \leq 0$, the asymptotic form of EA_2 is given by

$$\lim_{\tilde{\tau}_0 \rightarrow 0} \Delta S_A^{(2)}(\tilde{t}) = \begin{cases} \log N & , \quad \tilde{t} \in [|\tilde{x}_0|, |\tilde{x}_0| + 1] , \\ 0 & , \quad \tilde{t} \notin [|\tilde{x}_0|, |\tilde{x}_0| + 1] . \end{cases} \quad (3.14)$$

The above result is physically intuitive: the operator is inserted at $(x_0, 0)$, emitting a right-moving quasi-particle (holomorphic part of the inserted operator) and left-moving quasi-particle (anti-holomorphic part) with same constant speed. These quasi-particles propagate

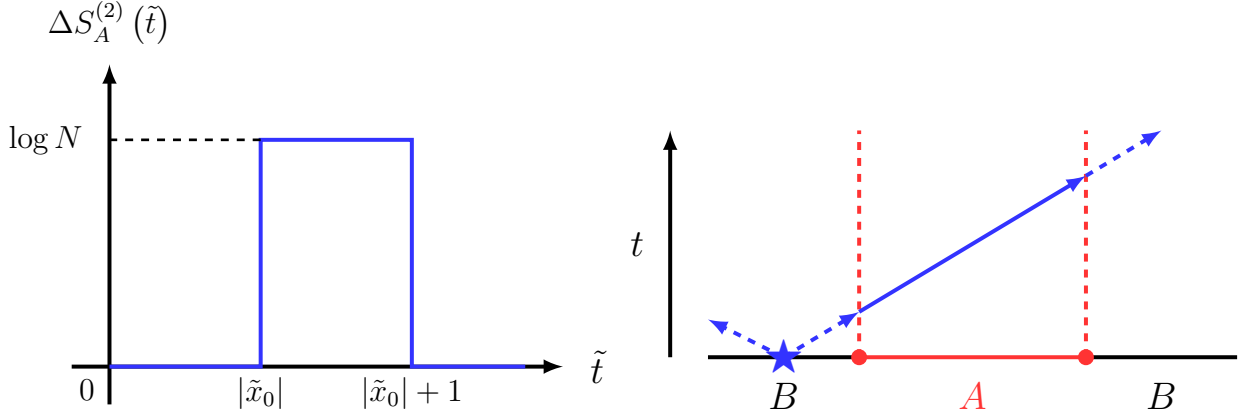


Figure 3: Real-time dependence of EA_2 for $\tilde{x}_0 < 0$ in the large interval limit $\tilde{\tau}_0 \rightarrow 0$ (left panel) and its quasi-particle interpretation (right panel). In the right panel, the symbol “ \star ” denotes the operator insertion point $(x_0, 0)$, and red line indicates the subregion A . The trajectories of the quasi-particles are depicted by the blue lines, and the horizontal and vertical axes represent space and real time directions, respectively.

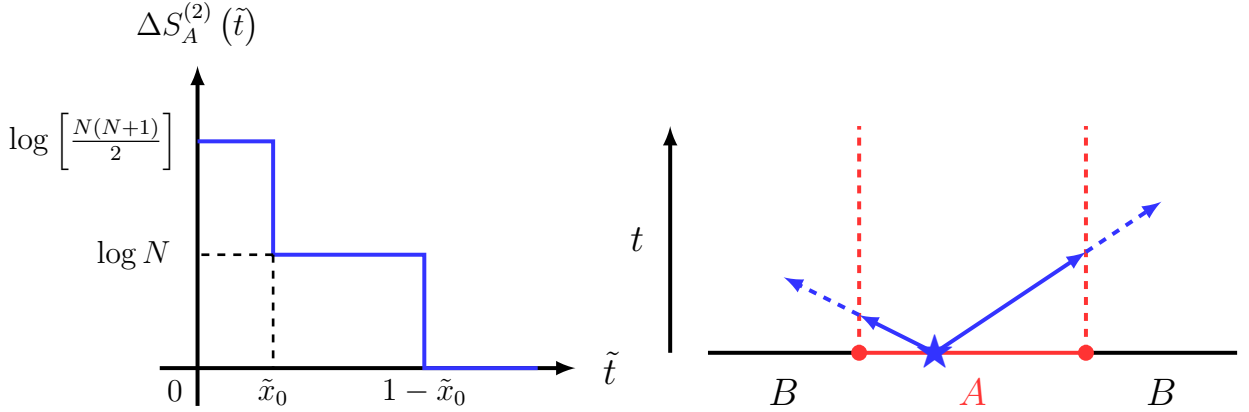


Figure 4: The real-time dependence of EA_2 for $\tilde{x}_0 > 0$ in the large interval limit $\tilde{\tau}_0 \rightarrow 0$ (left panel) and its quasi-particle interpretation (right panel). Here, we assume $\tilde{x}_0 < 1/2$ for simplicity.

in opposite directions to each other under the real-time evolution (see Fig. 3). When $\tilde{t} < |\tilde{x}_0|$, both quasi-particles remain outside the subregion A and thus do not break the symmetry there. At $\tilde{t} = |\tilde{x}_0|$, the right-moving quasi-particle enters subregion A and induces symmetry breaking in subregion A , yielding the non-zero value of EA_2 . Finally, when $\tilde{t} > |\tilde{x}_0| + 1$, the right-moving quasi-particle does no longer exist in the subregion A , and correspondingly EA_2 returns to zero.¹¹

¹¹A similar quasi-particle picture has been used in the context of entanglement entropy [56, 57], although in our case the quasi-particle and anti quasi-particle are not entangled to each other.

On the other hand, for $\tilde{x}_0 > 0$ we obtain

$$\lim_{\tilde{\tau}_0 \rightarrow 0} \Delta S_A^{(2)}(\tilde{t}) = \begin{cases} \log \left[\frac{N(N+1)}{2} \right] & , \quad 0 \leq \tilde{t} < \tilde{x}_0 , \\ \log N & , \quad \tilde{x}_0 \leq \tilde{t} < 1 - \tilde{x}_0 , \\ 0 & , \quad 1 - \tilde{x}_0 < \tilde{t} , \end{cases} \quad (3.15)$$

where we assume $\tilde{x}_0 < 1/2$ for simplicity. This result can be also understood from the viewpoint of the quasi-particle picture, as illustrated in Fig. 4. At $\tilde{t} = 0$, both quasi-particles are located at one point within the subregion A , and they lead symmetry breaking and the EA_2 takes the value of $\log [N(N+1)/2]$. For $\tilde{x}_0 \leq \tilde{t} < 1 - \tilde{x}_0$, the left-moving quasi-particle leaves subregion A while the right-moving quasi-particle remains inside. In this case, the quasi-particle leads weaker symmetry breaking and the EA_2 takes the value of $\log N$. Finally, for $1 - \tilde{x}_0 < \tilde{t}$, no quasi-particles remain in subregion A , and the EA_2 vanishes, indicating symmetry preservation.

We should also comment that our result is consistent with the intuition of the entanglement asymmetry. Roughly speaking, the entanglement asymmetry measures the effective degrees of freedom which break global symmetries in the subregion A . This intuitive feature can be explicitly seen in our result. Indeed, by taking the large N limit, the EA_2 given in (3.15) is reduced to

$$\lim_{\tilde{\tau}_0 \rightarrow 0} \Delta S_A^{(2)}(\tilde{t}) \stackrel{\text{Large } N}{=} \begin{cases} 2 \log N & , \quad 0 \leq \tilde{t} < \tilde{x}_0 , \\ \log N & , \quad \tilde{x}_0 \leq \tilde{t} < 1 - \tilde{x}_0 , \\ 0 & , \quad 1 - \tilde{x}_0 < \tilde{t} . \end{cases} \quad (3.16)$$

Clearly, the factor of 2 in front of the logarithm for $0 \leq \tilde{t} < \tilde{x}_0$ originates from the contributions of both left- and right-moving quasi-particles. In this regime, EA_2 is therefore twice as large as in the interval $\tilde{x}_0 \leq \tilde{t} < 1 - \tilde{x}_0$, where only the right-moving particle contributes. This behavior is fully consistent with the general intuition of the entanglement asymmetry.

As $\tilde{\tau}_0$ increases, the quasi-particle picture gradually loses its validity due to the finite size effect of the subregion A . In Fig. 5, we present the numerical evaluation of (3.9) for $\tilde{\tau}_0 = 0.01, 0.1, 0.2$. While the case $\tilde{\tau}_0 = 0.01$ is still well described by the quasi-particle picture, the results for $\tilde{\tau}_0 = 0.1$ and 0.2 exhibit smoother profiles, signaling the breakdown of this interpretation.

Other limits: $\tilde{\tau}_0 \rightarrow \infty$ **or** $|\tilde{x}_0| \rightarrow \infty$.

In these limits, the asymptotic form of EA_2 coincides with that in the long time limit (3.11), except that the parameter ϵ is replaced by

$$\begin{aligned} \epsilon &= \frac{1}{4} \left(\frac{1}{\tilde{\tau}_0} \right)^2 , \quad \tilde{\tau}_0 \rightarrow \infty , \\ \epsilon &= \frac{1}{4} \left(\frac{\tilde{\tau}_0}{\tilde{x}_0^2} \right)^2 , \quad |\tilde{x}_0| \rightarrow \infty . \end{aligned} \quad (3.17)$$

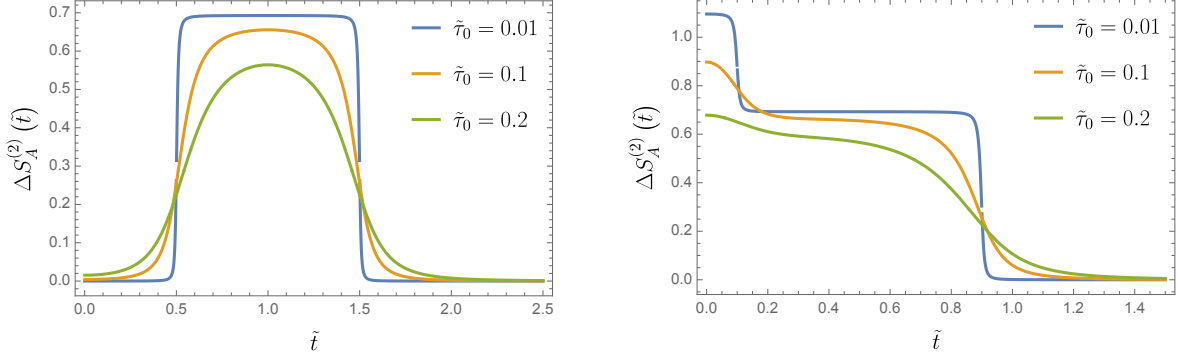


Figure 5: Numerical plot of EA_2 for $(N, k) = (2, 1)$ obtained from the analytical expression for $\tilde{\tau}_0 = 0.01, 0.1, 0.2$, plotted as a function of the dimensionless time \tilde{t} . The left panel corresponds to $\tilde{x}_0 = -0.5$ and the right panel to $\tilde{x}_0 = 0.1$. A smaller value of $\tilde{\tau}_0$ preserves the sharp feature predicted by the quasi-particle picture, while larger values smooth out the profiles.

In those cases, the insertion point of the symmetry-breaking operator is sufficiently far from subregion A . As a result, the operator insertion does not break the symmetry in subsystem A , thereby leading to a vanishing EA_2 .

3.3 Quantum Mpemba effect for $SU(N)$ symmetry

In the previous sections, we have studied various aspects of the EA_2 in $\widehat{su}(N)_k$ WZW model. We are now in a position to investigate the quantum Mpemba effect for $SU(N)$ symmetry via the EA_2 . To discuss the quantum Mpemba effect, we consider the two specific cases: $\tilde{x}_0 = 1/2, 0$ as illustrated in Fig. 6.

The coordinate $\tilde{\tau}_0$ describes the vertical separation between the operator insertion point and subregion A , and we treat $\tilde{\tau}_0$ as a parameter controlling the degrees of initial symmetry breaking. The EA_2 also depends on the real time \tilde{t} , rank N and level k , we thus express the EA_2 as $\Delta S_A^{(2)}(\tilde{t}; \tilde{x}_0, \tilde{\tau}_0, N, k)$. As shown in Fig. 7, the value of EA_2 at $\tilde{t} = 0$ decreases monotonically with respect to $\tilde{\tau}_0$ for any N and k :

$$\Delta S_A^{(2)}(\tilde{t} = 0; \tilde{x}_0, \tilde{\tau}_0, N, k) > \Delta S_A^{(2)}(\tilde{t} = 0; \tilde{x}_0, \tilde{\tau}'_0, N, k) \quad , \quad \tilde{\tau}_0 < \tilde{\tau}'_0 . \quad (3.18)$$

Increasing $\tilde{\tau}_0$ shifts the operator insertion points further away from subregion A , thereby reduces the degree of symmetry breaking.

On the other hand, from the long-time behavior of EA_2 in (3.11), increasing $\tilde{\tau}_0$ is equivalent to a larger ϵ , and all coefficients in front of ϵ are positive. As a result, EA_2 increases with $\tilde{\tau}_0$ in the limit $\tilde{t} \rightarrow \infty$:

$$\Delta S_A^{(2)}(\tilde{t} \rightarrow \infty; \tilde{x}_0, \tilde{\tau}_0, N, k) < \Delta S_A^{(2)}(\tilde{t} \rightarrow \infty; \tilde{x}_0, \tilde{\tau}'_0, N, k) \quad , \quad \tilde{\tau}_0 < \tilde{\tau}'_0 \ll \tilde{t}^2 . \quad (3.19)$$

Comparing the inequalities (3.18) and (3.19), we expect that the quantum Mpemba effect always occurs for $SU(N)$ symmetry. Fig. 8 shows the time evolution of the exact result (3.9)

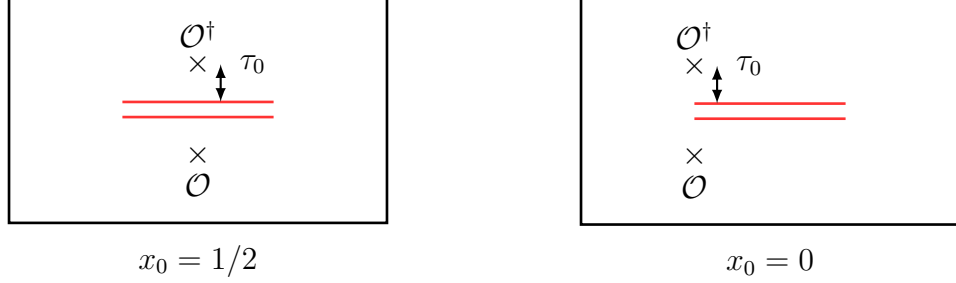


Figure 6: Our setup to discuss the quantum Mpemba effect . The red lines indicate the subregion A , while the symbols “ \times ” denote the insertion points of the operators \mathcal{O} and \mathcal{O}^\dagger . The spacial coordinate of the operator insertion is set to $\tilde{x}_0 = 1/2$ in the left panel and $\tilde{x}_0 = 0$ in the right panel. In both cases, the coordinate $\tilde{\tau}_0$ denotes the vertical distance between the operator insertion point and the subregion A .

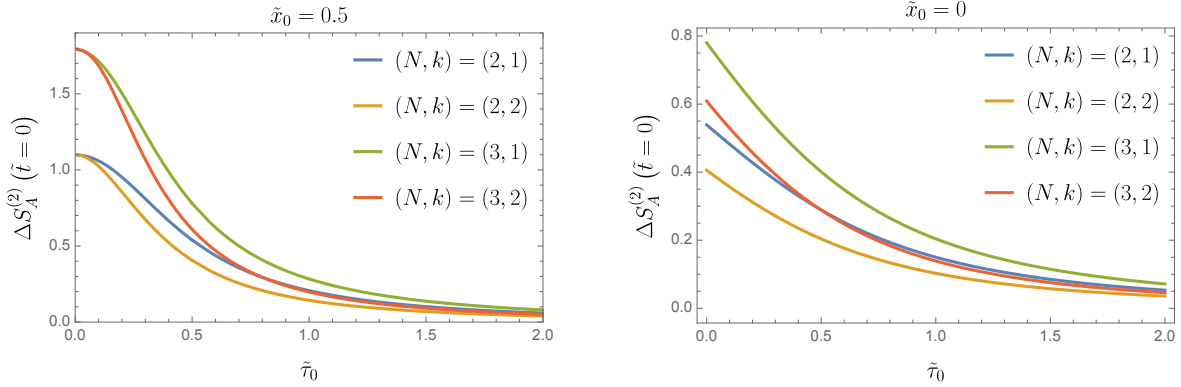


Figure 7: Numerical evaluation of EA_2 at $\tilde{t} = 0$, plotted as a function of $\tilde{\tau}_0$. The special coordinate of the operator insertion is chosen as $\tilde{x}_0 = 1/2$ in the left panel and $\tilde{x}_0 = 0$ in the right panel.

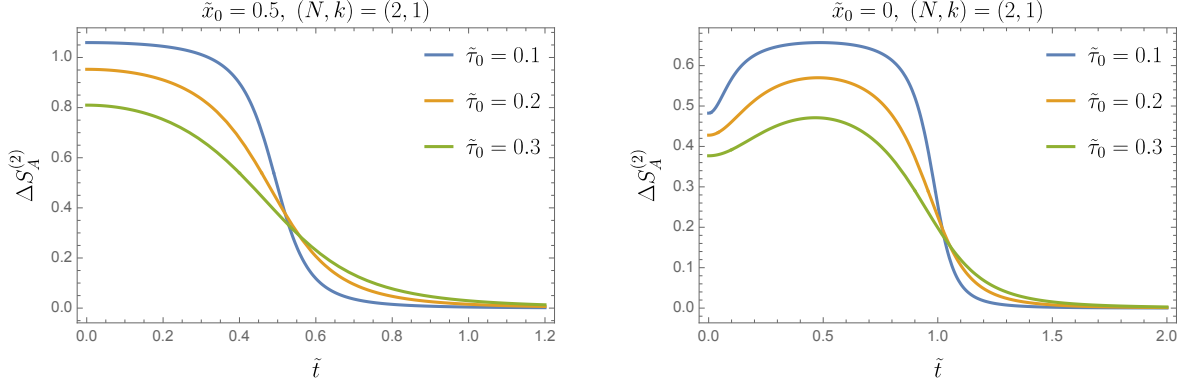


Figure 8: Time evolution of EA_2 for $\tilde{x}_0 = 1/2$ (left panel) and $\tilde{x}_0 = 0$ (right panel), with $(N, k) = (2, 1)$. In both cases, the curve exhibit crossings, indicating the presence of quantum Mpemba effect.

setting $(N, k) = (2, 1)$ and $\tilde{x}_0 = 1/2, 0$. For $\tilde{x}_0 = 1/2$, the EA_2 decreases monotonically and there is crossings in the plots, which is an evidence for the quantum Mpemba effect. On the other hand, in the case $\tilde{x}_0 = 0$, the EA_2 increases at early time,¹² however it eventually decreases monotonically for large \tilde{t} . We can observe crossings again and the quantum Mpemba effect occurs even for $\tilde{x}_0 = 0$. We can see that a similar behavior is found for other values of (N, k) although we do not show the corresponding numerical plots.

3.4 New type of quantum Mpemba effect

In the previous subsection, we analyzed the quantum Mpemba effect for $SU(N)$ symmetry by varying the parameter $\tilde{\tau}_0$ at fixed (N, k) . Here, we investigate the symmetry restoration structures by varying (N, k) while keeping $\tilde{\tau}_0$ fixed. Interestingly, we uncover a qualitatively new type of quantum Mpemba effect: increasing N amplifies the degree of initial symmetry breaking simultaneously accelerates the symmetry restoration, whereas increasing k diminishes the initial symmetry breaking and decelerates the symmetry restoration.

N dependence with k fixed

Let us first examine the N dependence of EA_2 with the level k fixed. From the long time behavior in (3.11), we obtain the following inequality for EA_2 between different values of N :

$$\Delta S_A^{(2)}(\tilde{t} \rightarrow \infty; \tilde{x}_0, \tilde{\tau}_0, N, k) > \Delta S_A^{(2)}(\tilde{t} \rightarrow \infty; \tilde{x}_0, \tilde{\tau}_0, N', k) \quad , \quad N < N' < k \quad (3.20)$$

¹²This behavior is consistent with the left panel in Fig. 5.

We next consider the N dependence of EA_2 at $\tilde{t} = 0$. In the long interval limit $\tilde{\tau}_0 \rightarrow 0$, (3.14) and (3.15) yield the initial value of EA_2 as¹³

$$\lim_{\tilde{\tau}_0 \rightarrow 0} \Delta S_A^{(2)}(\tilde{t} = 0; \tilde{x}_0, \tilde{\tau}_0, N, k) = \begin{cases} \log [N(N+1)/2] & \text{for } \tilde{x}_0 = 1/2 \\ \log N & \text{for } \tilde{x}_0 = 0 \end{cases} \quad (3.21)$$

which implies that the following inequality holds for arbitrary $k > 0$:

$$\Delta S_A^{(2)}(\tilde{t} = 0; \tilde{x}_0 = 1/2, 0, \tilde{\tau}_0 \rightarrow 0, N, k) < \Delta S_A^{(2)}(\tilde{t} = 0; \tilde{x}_0 = 1/2, 0, \tilde{\tau}_0 \rightarrow 0, N', k), \quad N < N'. \quad (3.22)$$

Comparing the inequalities (3.20) and (3.22), we expect that the initial value of EA_2 for small $\tilde{\tau}_0$ increases with N , while as enough time passes, it decreases with N for $N < k$. This behavior signals a new type of quantum Mpemba effect: increasing N amplifies the degree of initial symmetry breaking while accelerates symmetry restoration. In Fig. 9, we show the time evolution of EA_2 for various N with k fixed, in the cases $\tilde{x}_0 = 1/2$ and $\tilde{x}_0 = 0$ with $\tilde{\tau}_0 = 0.1$. As seen in the figures, the curves for $N < k$ exhibit crossings, indicating the new type of quantum Mpemba effect, whereas no crossings appear for $N > k$. In the plots, we present $(N, k) = (5, 30), (10, 30), (20, 30), (2, 1), (4, 1), (8, 1)$, but qualitatively similar behavior is observed for other values of (N, k) .

k dependence with N fixed

Let us now examine the k dependence of EA_2 with N fixed. From the long time behavior of EA_2 in (3.11), we obtain the following inequality between different values of k :

$$\Delta S_A^{(2)}(\tilde{t} \rightarrow \infty; \tilde{x}_0, \tilde{\tau}_0, N, k) < \Delta S_A^{(2)}(\tilde{t} \rightarrow \infty; \tilde{x}_0, \tilde{\tau}_0, N, k') \quad , \quad N < k < k'. \quad (3.23)$$

On the other hand, around the initial time $\tilde{t} = 0$, the k dependence in the EA_2 appears through the next leading term:

- $\tilde{x}_0 = 1/2$ and $N < k$.

$$\begin{aligned} \Delta S_A^{(2)}(\tilde{t} = 0; \tilde{x}_0, \tilde{\tau}_0, N, k) \\ = \log \left[\frac{N(N+1)}{2} \right] - \frac{(N-1)(N^2+2N-2)}{2N} c_{N,k} (4\tilde{\tau}_0^2)^{\frac{2N}{N+k}} + \mathcal{O}(\tilde{\tau}_0^2) \quad , \end{aligned} \quad (3.24)$$

where the coefficient $c_{N,k}$ is given in (3.13).

- $\tilde{x}_0 = 0$ and $N < k$.

$$\Delta S_A^{(2)}(\tilde{t} = \tilde{\delta}; \tilde{x}_0, \tilde{\tau}_0, N, k) = \log N - d_{N,k} \left(\frac{\tilde{\tau}_0}{2\tilde{\delta}} \right)^{\frac{N}{N+k}} + \mathcal{O} \left(\frac{\tilde{\tau}_0}{2\tilde{\delta}} \right) \quad , \quad (3.25)$$

¹³Strictly speaking, for $\tilde{x}_0 = 0$, one must slightly shift the time to $\tilde{t} = \tilde{\delta}$ and take $\tilde{\tau}_0 \ll \tilde{\delta}$. For a detailed derivation, see Appendix B.

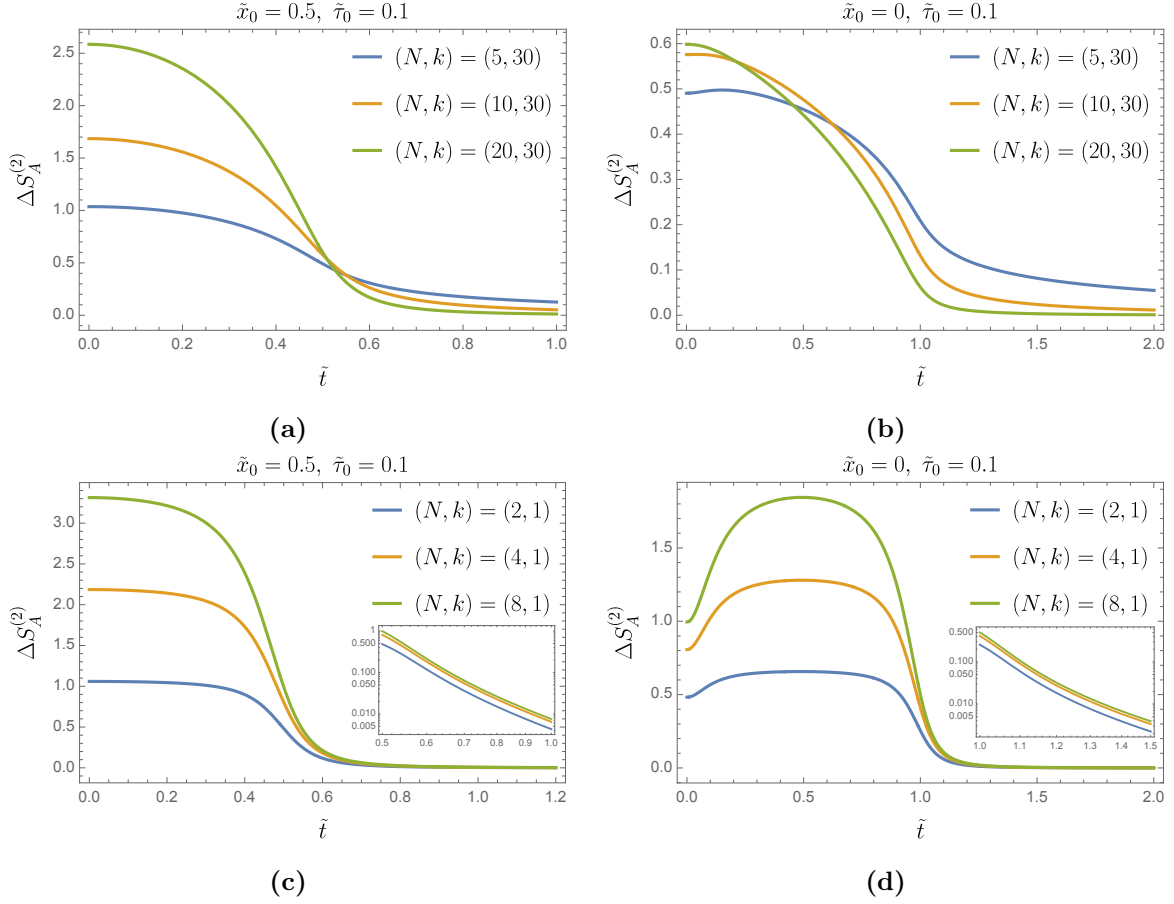


Figure 9: Time evolution of EA_2 for $\tilde{x}_0 = 1/2$ in panels (a), (c), and for $\tilde{x}_0 = 0$ in the panels (b) and (d). Panels (a) and (b) correspond to $N < k$, while panels (c) and (d) correspond to $k < N$. In the panels (c) and (d), we also show the logarithmic plot at intermediate time. For $N < k$, the curves exhibit crossings, indicating the presence of a new type of quantum Mpemba effect. In contrast, for $k < N$, we cannot find any crossings.

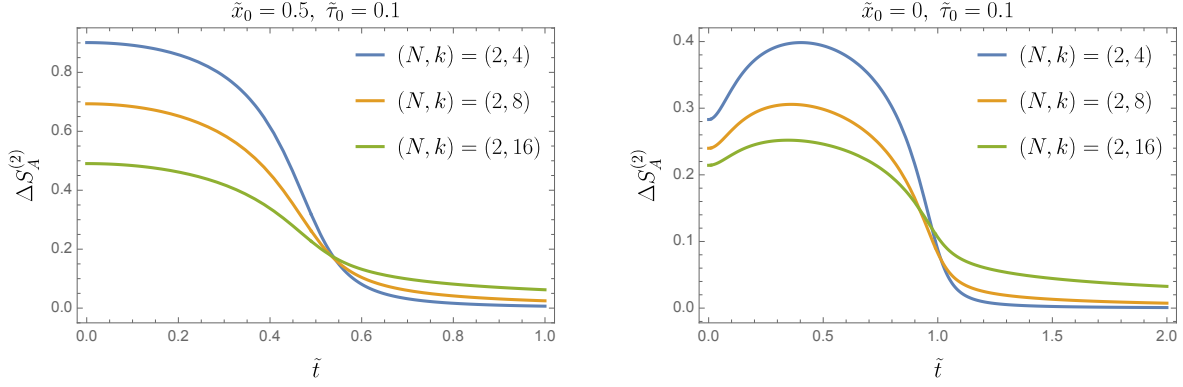


Figure 10: Time evolution of EA_2 for $\tilde{x}_0 = 1/2$ (left panel) and $\tilde{x}_0 = 0$ (right panel) with $N < k$ and $\tilde{\tau}_0 = 0.1$. In both cases, the curves exhibit crossings, indicating the presence of a new type of quantum Mpemba effect.

where $\tilde{\delta}$ is small parameter such that $\tilde{\tau}_0 \ll \tilde{\delta}$, and the coefficient $d_{N,k}$ is defined as

$$d_{N,k} = \frac{N(N-1)}{N+1} \frac{\Gamma\left(\frac{1}{N+k}\right) \Gamma\left(1 - \frac{1}{N+k}\right) \Gamma\left(\frac{k}{N+k}\right)}{\Gamma\left(\frac{k-1}{N+k}\right) \Gamma\left(\frac{k+1}{N+k}\right) \Gamma\left(\frac{N}{N+k}\right)}. \quad (3.26)$$

Note that $d_{N,k}$ is positive for $k \geq 2$ and vanishes for $k = 1$. A detailed derivation of these expressions is found in Appendix B.

In both cases, we find that EA_2 decreases as k increases for $N < k < k'$:

$$\Delta S_A^{(2)}(\tilde{t} = +0; \tilde{x}_0 = 1/2, 0, \tilde{\tau}_0 \rightarrow 0, N, k) > \Delta S_A^{(2)}(\tilde{t} = +0; \tilde{x}_0 = 1/2, 0, \tilde{\tau}_0 \rightarrow 0, N, k') . \quad (3.27)$$

Comparing the inequalities (3.23) and (3.27) we expect that increasing k diminishes the degree of initial symmetry breaking while decelerates symmetry restoration, which is another new type of quantum Mpemba effect. In Fig. 10, we present the time evolution of EA_2 for various k with N fixed, for $\tilde{x}_0 = 1/2$ and $\tilde{x}_0 = 0$ with $\tilde{\tau}_0 = 0.1$. As seen in the figures, the curves for $N < k$ exhibit crossings, indicating new type of quantum Mpemba effect. Although we show the plots for $(N, k) = (2, 4), (2, 8), (2, 16)$, qualitatively similar behavior is observed for other (N, k) .

Special case: $k = N$

So far, we have investigated the N and k dependencies of EA_2 independently. There, we found new types of quantum Mpemba effects which admit only a single crossing. Here, we consider the case of $N = k$. Interestingly, in this case, we can observe a symmetry restoration structure that allows for double crossings.¹⁴ In this case, the long time behavior (3.11) of

¹⁴Some examples where such multiple crossings occur are given in [17].

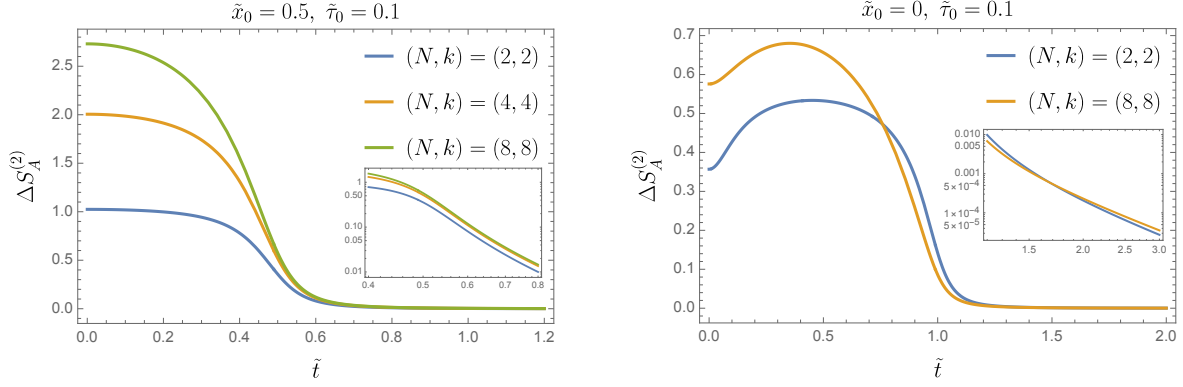


Figure 11: Time evolution of EA_2 for $\tilde{x}_0 = 1/2$ (left panel) and $\tilde{x}_0 = 0$ (right panel) with $N = k$ and $\tilde{\tau}_0 = 0.1$. In both panels, we also show the logarithmic plot of the long time behavior. For $\tilde{x}_0 = 1/2$, the curves show no crossings, indicating the absence of the quantum Mpemba effect. In contrast, for $\tilde{x}_0 = 0$, the curves exhibit double crossings.

EA_2 is given by

$$\Delta S_A^{(2)}(\tilde{t} \rightarrow \infty; \tilde{x}_0, \tilde{\tau}_0, N, N) = \left(1 - \frac{2}{N(N+1)}\right) \cdot \frac{1}{4} \left(\frac{\tilde{\tau}_0}{\tilde{t}^2}\right)^2 + \mathcal{O}\left(\left(\frac{\tilde{\tau}_0}{\tilde{t}^2}\right)^4\right), \quad (3.28)$$

which implies

$$\Delta S_A^{(2)}(\tilde{t} \rightarrow \infty; \tilde{x}_0, \tilde{\tau}_0, N, N) < \Delta S_A^{(2)}(\tilde{t} \rightarrow \infty; \tilde{x}_0, \tilde{\tau}_0, N', N') \quad , \quad N < N' \quad (3.29)$$

From (3.21), we also find that the EA_2 increase with N around $\tilde{t} = 0$:

$$\Delta S_A^{(2)}(\tilde{t} = +0; \tilde{x}_0 = 1/2, 0, \tilde{\tau}_0 \rightarrow 0, N, N) < \Delta S_A^{(2)}(\tilde{t} = +0; \tilde{x}_0 = 1/2, 0, \tilde{\tau}_0 \rightarrow 0, N', N') \quad . \quad (3.30)$$

From the inequalities (3.29) and (3.30), we see that either no crossing or an even number crossings are allowed. In Fig. 11, we present the time evolution of EA_2 for $\tilde{x}_0 = 1/2$ and $\tilde{x}_0 = 0$ with $\tilde{\tau}_0 = 0.1$. As shown in the figure, the curves for $\tilde{x}_0 = 1/2$ do not exhibit any crossings, indicating the absence of the quantum Mpemba effect. In contrast, the plot for $\tilde{x}_0 = 0$ exhibits the double crossing. We comment that similar behaviors can be found for other values of $k = N$.

4 Quantum Mpemba effect: adjoint case

So far, we have explored the symmetry restoration structures focusing on the initial state constructed from the primary operator in the fundamental representation. It is then natural to ask if the phenomena observed in the previous section are modified or not when the initial

state is built from primaries in other representations. To answer this question, in what follows, we consider the initial state constructed from the WZW current $J^a(z, \bar{z})$:¹⁵

$$|\psi\rangle = \frac{1}{\sqrt{Z_0}} J^a(z_-, \bar{z}_-) |0\rangle, \quad J^a(z_-, \bar{z}_-) \equiv J^a(z_-) \otimes \bar{J}^a(\bar{z}_-). \quad (4.1)$$

To derive EA₂ for the above initial state, we need the following four-point function of the WZW currents:

$$F^{abcd}(x) \equiv \langle J^a(x) J^b(0) J^c(1) J^d(\infty) \rangle. \quad (4.2)$$

Using the operator product expansion between the WZW currents, one can compute this four-point function [58]:

$$F^{abcd}(x) = k^2 \left[\frac{\delta^{ab} \delta^{cd}}{x^2} + \frac{\delta^{ac} \delta^{bd}}{(1-x)^2} + \delta^{ad} \delta^{bc} \right] + \frac{k}{3} \left[\frac{C_1^{abcd}}{x(1-x)} + \frac{C_2^{abcd}}{x} + \frac{C_3^{abcd}}{1-x} \right]. \quad (4.3)$$

where C_i^{abcd} is defined in terms of the structure constant f_{abc} of SU(N)

$$\begin{aligned} C_1^{abcd} &\equiv f^{abe} f^{cde} + f^{ace} f^{bde}, \\ C_2^{abcd} &\equiv f^{abe} f^{cde} + f^{ade} f^{cbe}, \\ C_3^{abcd} &\equiv f^{ace} f^{bde} + f^{ade} f^{bce}. \end{aligned} \quad (4.4)$$

Moreover, the WZW current J^a transforms under $g \in \text{SU}(N)$ as

$$J'^a(z) = \sum_b [D(g)]^{ba} J^b, \quad D(g)^{ab} = 2\text{Tr}(g^\dagger t^a g t^b), \quad (4.5)$$

where t^a is the generator of SU(N), and the trace is normalized to $\text{Tr}(t^a t^b) = \frac{1}{2} \delta^{ab}$. Repeating a similar analysis to that in Section 2, we obtain the following expression for the EA₂:

$$\Delta S_A^{(2)}(t) = -\log \left[\sum_{b,b',c,c'} \int_{\text{SU}(N)} dg D(g)^{ba} D(g)^{ca} D(g)^{b'a} D(g)^{c'a} \frac{F^{abac}(t) \bar{F}^{ab'ac'}(t)}{F^{aaaa}(t) \bar{F}^{aaaa}(t)} \right], \quad (4.6)$$

where $F^{abcd}(t) \equiv F^{abcd}(x(t))$, $\bar{F}^{abcd}(t) \equiv F^{abcd}(\bar{x}(t))$ and the time-dependence of cross-ratios are given in (2.34) and (2.35). Employing the Haar integral formula [59, 60]:¹⁶

$$\int_{\text{SU}(N)} dg D(g)^{ba} D(g)^{ca} D(g)^{b'a} D(g)^{c'a} = \frac{1}{N^4 - 1} (\delta_{bc} \delta_{b'c'} + \delta_{bb'} \delta_{cc'} + \delta_{bc'} \delta_{cb'}), \quad (4.7)$$

we obtain the following expression.

$$\Delta S_A^{(2)}(t) = -\log \left[\frac{(\sum_b F^{abab}(t)) (\sum_b \bar{F}^{abab}(t)) + 2 \sum_{b,c} F^{abac}(t) \bar{F}^{abac}(t)}{(N^4 - 1) F^{aaaa}(t) \bar{F}^{aaaa}(t)} \right]. \quad (4.8)$$

¹⁵We can straightforwardly generalize the discussion to the non-diagonal case. See also footnote 9.

¹⁶The easiest way to understand this integral formula is to use the fact that the matrix $D(g)$ furnishes the fundamental representation of SO($N^2 - 1$).

One can readily check that the EA_2 exactly vanishes in the limit $t \rightarrow \infty$:

$$\lim_{t \rightarrow \infty} \Delta S_A^{(2)}(t) = 0 , \quad (4.9)$$

which means that, at the level of subsystem A , the global symmetry $\text{SU}(N)$ is preserved at late times. For simplicity, in the remainder of this section, we restrict ourselves to the large k limit, where the second term in the RHS of (4.3) can be dropped. In this limit, the EA_2 does not depend on k , and has the following simplified form:

$$\Delta S_A^{(2)}(\tilde{t}; \tilde{x}_0, \tilde{\tau}_0, N) = -\log \left[\frac{(N^4 - 1)f_1(x, \bar{x}) + (N^2 + 1)f_2(x, \bar{x}) + 3f_3(x, \bar{x})}{(N^4 - 1)(1 - x + x^2)^2(1 - \bar{x} + \bar{x}^2)} \right] , \quad (4.10)$$

where $x = x(t)$, $\bar{x} = \bar{x}(t)$, and $f_i(x, \bar{x})$ are defined as

$$\begin{aligned} f_1(x, \bar{x}) &= x^2 \bar{x}^2 , \\ f_2(x, \bar{x}) &= x^2(1 - \bar{x})^2(1 + \bar{x}^2) + \bar{x}^2(1 - x)^2(1 + x^2) , \\ f_3(x, \bar{x}) &= (1 - x)^2(1 - \bar{x})^2(1 + x^2 + \bar{x}^2 + x^2 \bar{x}^2) . \end{aligned} \quad (4.11)$$

Also, the time dependence of the cross-ratios are explicitly given in (2.34) and (2.35). As in the previous section, we summarize the asymptotic behaviors of EA_2 in the long time limit and large interval limit:

- **Long time limit:** $\tilde{t} \rightarrow \infty$.

$$\Delta S_A^{(2)}(\tilde{t}; \tilde{x}_0, \tilde{\tau}_0, N) = \frac{1}{4} \left(1 - \frac{1}{N^2 - 1} \right) \left(\frac{\tilde{\tau}_0}{\tilde{t}^2} \right)^4 + \mathcal{O} \left(\left(\frac{\tilde{\tau}_0}{\tilde{t}^2} \right)^6 \right) . \quad (4.12)$$

- **Large interval limit:** $\tilde{\tau}_0 \rightarrow 0$.

- (i) $\tilde{x}_0 = 1/2$.

$$\Delta S_A^{(2)}(\tilde{t} = 0; \tilde{x}_0, \tilde{\tau}_0, N) = \log \left[\frac{N^4 - 1}{3} \right] - \frac{32}{3} (N^2 - 1) \tilde{\tau}_0^4 + \mathcal{O}(\tilde{\tau}_0^6) , \quad (4.13)$$

- (ii) $\tilde{x}_0 = 0$.

$$\Delta S_A^{(2)}(\tilde{t} = \tilde{\delta}; \tilde{x}_0, \tilde{\tau}_0, N) = \log [N^2 - 1] - \frac{(N^2 - 2)(N^2 - 1)}{N^2 + 1} \left(\frac{\tilde{\tau}_0}{2\tilde{\delta}} \right)^4 + \mathcal{O} \left(\left(\frac{\tilde{\tau}_0}{2\tilde{\delta}} \right)^6 \right) . \quad (4.14)$$

We make a comment on the asymptotic behavior (4.14). The leading term in (4.14) is equivalent to the logarithm of the dimension of the adjoint representation of $\text{SU}(N)$. Together with the fundamental case, where the leading contribution is $\log N$ as (3.25), this strongly

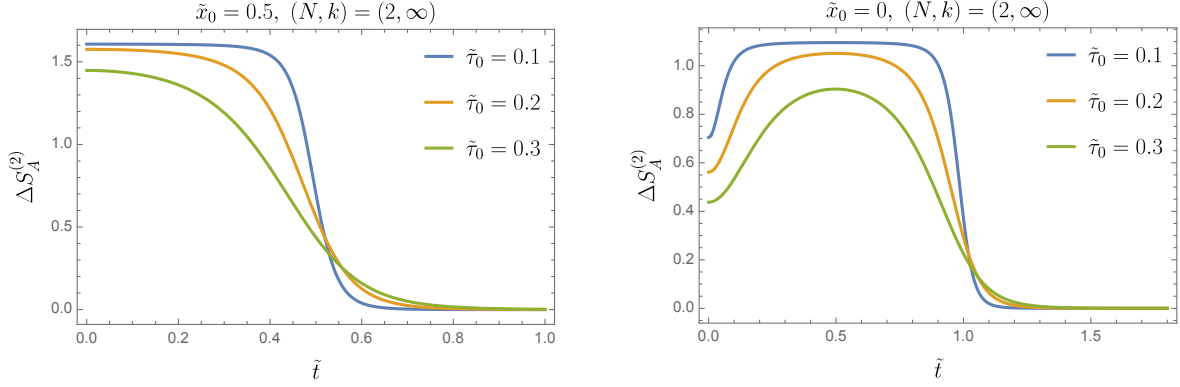


Figure 12: Time evolution of EA_2 constructed from currents for $\tilde{x}_0 = 1/2$ (left panel) and $\tilde{x}_0 = 0$ (right panel), with $(N, k) = (2, \infty)$. In both cases, the curves exhibit crossings, indicating the presence of quantum Mpemba effect.

suggests that, in general, the leading term is given by the logarithm of the dimension of the representation associated with the operator that prepares the initial state.

We now investigate the quantum Mpemba effect using (4.10). Firstly, fixing the rank N and varying the parameter $\tilde{\tau}_0$, we obtain the following inequalities from the above asymptotic behaviors:

$$\begin{cases} \Delta S_A^{(2)}(\tilde{t} = +0; \tilde{x}_0 = 1/2, 0, \tilde{\tau}_0 \rightarrow 0, N) > \Delta S_A^{(2)}(\tilde{t} = +0; \tilde{x}_0 = 1/2, 0, \tilde{\tau}'_0 \rightarrow 0, N) \\ \Delta S_A^{(2)}(\tilde{t} \rightarrow \infty; \tilde{x}_0, \tilde{\tau}_0, N) < \Delta S_A^{(2)}(\tilde{t} \rightarrow \infty; \tilde{x}_0, \tilde{\tau}'_0, N) \end{cases}, \quad \tilde{\tau}_0 < \tilde{\tau}'_0. \quad (4.15)$$

Note that we have already seen the same inequalities as these ones in (3.18) and (3.19). We therefore expect the quantum Mpemba effect to occur here as well. Fig. 12 presents the time evolution of the result (4.10) for $N = 2$ and $\tilde{x}_0 = 1/2, 0$. Indeed, the curves clearly exhibit crossings, providing evidence of the quantum Mpemba effect. Similar quantitative behavior is observed for other values of N .

On the other hand, we find no evidence of the new type of quantum Mpemba effect in the current case. Indeed, the asymptotic behaviors (4.12), (4.13) and (3.25) imply that for $\tilde{x}_0 = 1/2, 0$,

$$\begin{cases} \Delta S_A^{(2)}(\tilde{t} = +0; \tilde{x}_0, \tilde{\tau}_0 \rightarrow 0, N) < \Delta S_A^{(2)}(\tilde{t} = +0; \tilde{x}_0, \tilde{\tau}_0 \rightarrow 0, N') \\ \Delta S_A^{(2)}(\tilde{t} \rightarrow \infty; \tilde{x}_0, \tilde{\tau}_0, N) < \Delta S_A^{(2)}(\tilde{t} \rightarrow \infty; \tilde{x}_0, \tilde{\tau}_0, N') \end{cases}, \quad N < N'. \quad (4.16)$$

which forbids an odd number of crossings in the time evolution of EA_2 . Fig. 13 shows the time evolution of EA_2 for various N with $\tilde{x}_0 = 1/2, 0$ and $\tilde{\tau}_0 = 0.1$. As evident from the figures, no crossings occur, indicating the absence of the quantum Mpemba effect. Similar behavior is observed for other values of N .

In summary, we analyzed the EA_2 constructed from currents in the adjoint representation. While the standard quantum Mpemba effect is observed, we are not able to find the new type of quantum Mpemba effect in this case.

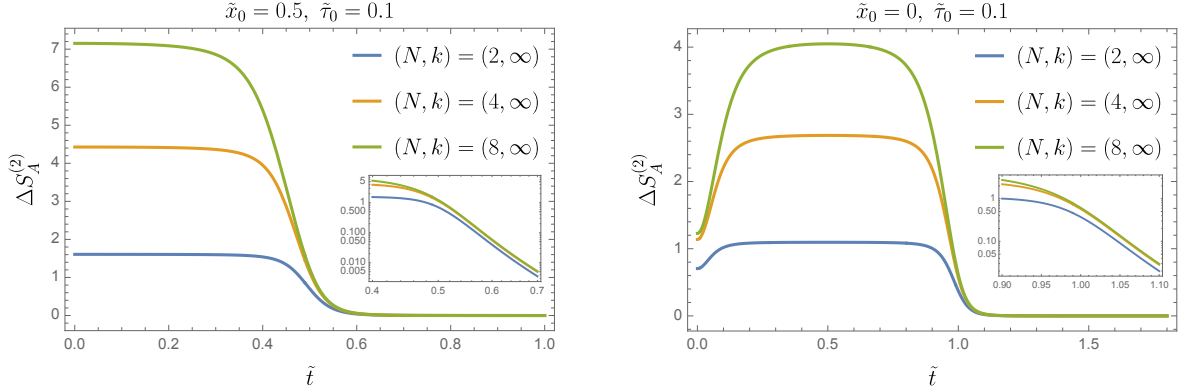


Figure 13: Time evolution of EA_2 constructed from currents for $\tilde{x}_0 = 1/2$ (left panel) and $\tilde{x}_0 = 0$ (right panel) with $\tilde{\tau}_0 = 0.1$. In both cases, the curves exhibit no crossings, indicating the absence of quantum Mpemba effect.

5 Conclusion and discussion

In this paper, we presented the first systematic study of symmetry restoration of non-Abelian symmetries by using the $\widehat{su}(N)_k$ WZW model. Due to the Coleman-Mermin-Wagner theorem, spontaneous breaking of continuous global symmetries is forbidden in $1+1$ dimensions. We therefore prepared excited initial states constructed from the primary operator in fundamental representation and the WZW current, both of which explicitly break the global symmetry $SU(N)$. In Section 2, we derived the general form of EA_2 for arbitrary initial states, which is given in (2.36). In the derivation, we used the conformal symmetry to express EA_2 in terms of four-point function. In Section 3, we applied the general formula for EA_2 to the case where the initial state is created by the primary operator in the fundamental representation, and investigated its time evolution. We confirmed that the quantum Mpemba effect, which is the phenomenon that the state with stronger initially symmetry breaking relaxes more rapidly, also occurs for the global symmetry $SU(N)$. Furthermore, we uncovered a new type of quantum Mpemba effect: increasing the rank N amplifies the degree of initial symmetry breaking, while accelerating the symmetry restoration. Conversely, increasing the level k weakens the degree of initial symmetry breaking while decelerating the symmetry restoration. In Section 4, as another representation, we also studied how the initially broken global symmetry is restored by employing the initial state built from the WZW current. We take the large k limit, and see that this limit simplifies the expression of EA_2 . In this case, we find that the quantum Mpemba effect always occurs at fixed rank N , but no evidence for the new type of quantum Mpemba effect was observed.

This work opens several interesting directions for future studies, and some of them are listed as follows.

- Firstly, it is interesting to extend our analysis to the other representations and study whether a new type of quantum Mpemba effects occur or not. This leads to more well-

understanding of symmetry restoration for non-Abelian global symmetries. Although our analysis focused on $\widehat{su}(N)_k$ symmetry, it can be straightforwardly extended to other affine Lie algebras. For instance, the explicit forms of four-point correlations of two-fundamental and two anti-fundamental primaries are known for $\widehat{so}(N)_k$ and $\widehat{sp}(N)_k$ symmetries [61, 62], and thus our approach can be directly applied to these cases.

- Another interesting direction is to explore finite temperature systems. It is known that the Rényi entanglement entropy at low temperature can be expressed in terms of correlation functions [54, 63–65]. This analysis can be extended to the Rényi entanglement asymmetry, making it intriguing to investigate how thermal effects contribute to the quantum Mpemba effect through symmetry restoration.
- It would be valuable to interpret our result from the perspective of three-dimensional Chern-Simons theory, which is dual to the WZW model [66]. In our analysis, we saw that the new type of quantum Mpemba effects occurs only for fundamental primary, but not for adjoint primary. It is interesting to explore some implications of our results from the three-dimensional perspective.

Acknowledgments

The work of H.F. and S.S. was supported by Grant-in-Aid for JSPS fellows, Grant Nos. 24KJ1637 and 23KJ1533, respectively.

A Four-point function in Wess-Zumino-Witten models

In this appendix, we present the review on how we can determine the four-point functions in the $\widehat{su}(N)_k$ WZW model by solving the Knizhnik-Zamolodchikov (KZ) equation. We follow the notation used in [67].

A.1 Preliminary

Before delving into the details, for completeness, it is convenient to recap the basics of WZW models whose affine Lie algebra is given by $\widehat{\mathfrak{g}}_k$. Let Φ_Λ^α is the primary field in the irreducible module of the highest weight Λ with weight α , and its conformal dimension h_Λ is given by

$$h_\Lambda = \frac{(\Lambda, \Lambda + 2\rho)}{2(k + g)} . \quad (\text{A.1})$$

Here, ρ is the Weyl vector which is defined in terms of the fundamental weights $\{w_i\}$ as

$$\rho \equiv \sum_i w_i . \quad (\text{A.2})$$

Also, g is the dual Coxeter number of the Lie algebra \mathfrak{g} . In general, all representations can be expanded in terms of the fundamental weights:

$$\Lambda = \sum_i \lambda_i w_i, \quad \lambda_i \in \mathbb{Z}, \quad (\text{A.3})$$

where the set of the coefficients is referred to as the Dynkin label. It is convenient to introduce the quadratic form matrix F_{ij} which is the inner product between fundamental weights:

$$F_{ij} \equiv (w_i, w_j). \quad (\text{A.4})$$

Then, by plugging (A.2) and (A.3) into (A.1), we can rewrite the conformal dimension h_Λ in terms of the Dynkin label and quadratic form matrix.

A.2 Knizhnik-Zamolodchikov equation

Let us consider the following four-point function:¹⁷

$$\mathcal{F}_{\alpha_1 \alpha_4}^{\alpha_2 \alpha_3}(z_i) := \langle \Phi_{\Lambda_1, \alpha_1}(z_1) \Phi_{\Lambda_2}^{\alpha_2}(z_2) \Phi_{\Lambda_3}^{\alpha_3}(z_3) \Phi_{\Lambda_4, \alpha_4}(z_4) \rangle, \quad (\text{A.5})$$

where $\Phi_{\Lambda_i, \alpha_i}$ is the primary operator in the representation Λ_i , and $\alpha_i = 1, 2, \dots, \dim \Lambda_i$. By using the conformal transformation, we can always map the four holomorphic coordinates (z_1, z_2, z_3, z_4) to $(x, 0, 1, \infty)$ with

$$x := \frac{z_{12} z_{34}}{z_{14} z_{32}}, \quad (\text{A.6})$$

where $z_{ij} := z_i - z_j$. Then, the above four-point function (A.5) can be rewritten as

$$\mathcal{F}_{\alpha_1 \alpha_4}^{\alpha_2 \alpha_3}(z_i) = (z_{14} z_{23})^{-2h} F_{\alpha_1 \alpha_4}^{\alpha_2 \alpha_3}(x), \quad (\text{A.7})$$

where $F_{\alpha_1 \alpha_4}^{\alpha_2 \alpha_3}(x)$ is defined by

$$F_{\alpha_1 \alpha_4}^{\alpha_2 \alpha_3}(x) \equiv \langle \Phi_{\Lambda_1, \alpha_1}(x) \Phi_{\Lambda_2}^{\alpha_2}(0) \Phi_{\Lambda_3}^{\alpha_3}(1) \Phi_{\Lambda_4, \alpha_4}(\infty) \rangle. \quad (\text{A.8})$$

In order for the four-point function not to vanish, the tensor product of the four affine integrable representations of primary fields must contain at least one identity. Suppose that this tensor product takes the following form:

$$\Lambda_1 \otimes \Lambda_2 \otimes \Lambda_3 \otimes \Lambda_4 \supset m \mathbf{1}, \quad (\text{A.9})$$

where m is some positive integer. This implies that there are m invariant tensors $\{I_A\}$, and the four-point function can be decomposed as

$$F_{\alpha_1 \alpha_4}^{\alpha_2 \alpha_3}(x) = \sum_{A=1}^m F_A(x) (I_A)_{\alpha_1 \alpha_4}^{\alpha_2 \alpha_3}. \quad (\text{A.10})$$

¹⁷Here, we omit the anti-holomorphic part for simplicity.

Then, the four-point function (A.5) satisfies the following KZ equation [41]:

$$\left[\partial_{z_\alpha} - \frac{1}{k+g} \sum_{\beta \neq \alpha} \frac{\sum_a R_{\Lambda_\alpha}(t^a) \otimes R_{\Lambda_\beta}(t^a)}{z_\alpha - z_\beta} \right] (z_{14} z_{23})^{-2h} \sum_{A=1}^m I_A F_A(x) = 0 , \quad (\text{A.11})$$

where $R_{\Lambda_\alpha}(t^a)$ is the representation matrix of the generator t^a in the representation Λ_α . We should remark that we omit the indices for the representation space, and the generators $R_{\Lambda_\alpha}(t^a)$ act on the indices of the invariant tensor I_A properly. In particular, we set $\alpha = 1$, and the above KZ equation turns into

$$\left[\frac{-2h}{z_{14}} + \left(\frac{x}{z_{12}} - \frac{x}{z_{14}} \right) \partial_x - \frac{1}{k+g} \sum_{\beta \neq 1} \frac{\sum_a R_{\Lambda_1}(t^a) \otimes R_{\Lambda_\beta}(t^a)}{z_1 - z_\beta} \right] \sum_{A=1}^m I_A F_A(x) = 0 . \quad (\text{A.12})$$

At this stage, we set the four space-time coordinates as

$$z_1 = x , \quad z_2 = 0 , \quad z_3 = 1 , \quad z_4 = \infty , \quad (\text{A.13})$$

then the above differential equation is reduced to

$$\left[\partial_x - \frac{1}{k+g} \frac{\sum_a R_{\Lambda_1}(t^a) \otimes R_{\Lambda_2}(t^a)}{x} - \frac{1}{k+g} \frac{\sum_a R_{\Lambda_1}(t^a) \otimes R_{\Lambda_3}(t^a)}{x-1} \right] \sum_{A=1}^m I_A F_A(x) = 0 . \quad (\text{A.14})$$

A.3 Computing the four-point function for $\widehat{su}(N)_k$

In the following, we focus on the case $\hat{\mathfrak{g}}_k = \widehat{su}(N)_k$ and derive the four-point function. In (A.5), we specify the representations of the primary operators as follows. We take Λ_1 and Λ_4 to be in the fundamental representation \mathbf{N} , whose affine Dynkin labels are

$$\Lambda_1 = \Lambda_4 = \mathbf{N} : [\lambda_0; \lambda_1, \lambda_2, \dots, \lambda_{N-1}] = [k-1; 1, 0, 0, \dots, 0] . \quad (\text{A.15})$$

The conformal dimension h of this representation is

$$h = \frac{N^2 - 1}{2N(k+N)} . \quad (\text{A.16})$$

This expression follows directly from (A.1), using the fact that the dual Coxeter number is $g = N$ and that the quadratic form matrix is given by

$$F_{1j} = \frac{N-j}{N} . \quad (\text{A.17})$$

Similarly, we choose Λ_2 and Λ_3 to be in the anti-fundamental representation $\overline{\mathbf{N}}$, with affine Dynkin labels

$$\Lambda_2 = \Lambda_3 = \overline{\mathbf{N}} : [\lambda_0; \lambda_1, \lambda_2, \dots, \lambda_{N-1}] = [k-1; 0, 0, 0, \dots, 1] . \quad (\text{A.18})$$

Let Φ_i denote a primary operator in the fundamental representation ($i = 1, \dots, N$). The corresponding four-point function (A.8) is written as

$$F_{ik}^{j\ell}(x) := \langle \Phi_i(x) \Phi^{\dagger j}(0) \Phi^{\dagger \ell}(1) \Phi_k(\infty) \rangle . \quad (\text{A.19})$$

In our case, we have two invariant tensors¹⁸ (i.e., $m = 2$ in (A.9)) and the invariant tensors are explicitly given by

$$(I_1)_{ik}^{j\ell} = \delta_i^j \delta_k^\ell , \quad (I_2)_{ik}^{j\ell} = \delta_i^\ell \delta_k^j . \quad (\text{A.20})$$

Then, the KZ equation (A.14) reads

$$\sum_{A=1}^2 \left[(I_A)_{ik}^{j\ell} \partial_x + \frac{1}{k+g} \frac{T_{ip}^{qj}(I_A)_{qk}^{p\ell}}{x} + \frac{1}{k+g} \frac{T_{ip}^{q\ell}(I_A)_{qk}^{jp}}{x-1} \right] F_A(x) = 0 , \quad (\text{A.21})$$

where we restored the full indices for representations, and the tensor $T_{ik}^{j\ell}$ is given by

$$T_{ik}^{j\ell} = \delta_i^\ell \delta_k^j - \frac{1}{N} \delta_i^j \delta_k^\ell . \quad (\text{A.22})$$

Then, the KZ equations are equivalent to the following two differential equations:

$$\partial_x F_1 + \frac{1}{\kappa} \left(\frac{N^2 - 1}{N} \frac{F_1}{x} + \frac{F_2}{x} - \frac{1}{N} \frac{F_1}{x-1} \right) = 0 , \quad (\text{A.23})$$

$$\partial_x F_2 + \frac{1}{\kappa} \left(\frac{N^2 - 1}{N} \frac{F_2}{x-1} + \frac{F_1}{x-1} - \frac{1}{N} \frac{F_2}{x} \right) = 0 , \quad (\text{A.24})$$

where $\kappa \equiv k + N$. To solve these equations, we firstly express F_2 in terms of F_1 by using the first equation:

$$F_2 = -\kappa x \partial_x F_1 - \frac{N^2 - 1}{N} F_1 + \frac{1}{N} \frac{x}{x-1} F_1 . \quad (\text{A.25})$$

By substituting this into the second equation, one can obtain the second-order differential equation for F_1 . By rewriting F_1 as

$$F_1 = x^r (1-x)^s f_1(x) , \quad (\text{A.26})$$

this differential equation can be written as

$$x(1-x) \partial_x^2 f_1 + A(x) \partial_x f_1 + B(x) f_1 = 0 , \quad (\text{A.27})$$

¹⁸Precisely speaking, when $k = 1$, we have only one invariant tensor. This can be verified by using the representation theory of the affine Lie algebra. We will come back to this issue later again.

where $A(x)$ and $B(x)$ are given by

$$\begin{aligned}
\kappa N \cdot A(x) &\equiv (1-x)(2r\kappa N + N^2 - 2 + \kappa N) - x(2s\kappa N + N^2 - 2) , \\
(\kappa N)^2 \cdot B(x) &\equiv \frac{1-x}{x} (\kappa^2 N^2 r(r-1) + r\kappa N(N^2 - 2) + r\kappa^2 N^2 - (N^2 - 1)) \\
&\quad + \frac{x}{1-x} (\kappa^2 N^2 s(s-1) + s\kappa N(N^2 - 2) + \kappa N - (N^2 - 1)) \\
&\quad - 2rs\kappa^2 N^2 - (s+r)\kappa N(N^2 - 1) - s\kappa^2 N^2 + \kappa N - 1 - (N^2 - 1)^2 + N^2 .
\end{aligned} \tag{A.28}$$

Note that if $B(x)$ do not depend on the cross-ratio x , the solution f_1 can be written in terms of the hypergeometric function. This condition gives rise to non-trivial constraints on r and s . Indeed, by requiring that the terms which are proportional $(x/(1-x))^{\pm 1}$ in the function $B(x)$, r and s are fixed to be

$$r = r_+ \equiv \frac{1}{\kappa N} = h_{\hat{\theta}} - 2h \quad \text{or} \quad r = r_- \equiv -\frac{N^2 - 1}{\kappa N} = -2h , \tag{A.29}$$

$$s = s_+ \equiv \frac{1}{\kappa N} = h_{\hat{\theta}} - 2h \quad \text{or} \quad s = s_- \equiv 1 - \frac{N^2 - 1}{\kappa N} = 1 - 2h , \tag{A.30}$$

where h and $h_{\hat{\theta}}$ are the conformal dimensions of the chiral WZW primary fields in fundamental and adjoint representations. At first glance, we have four solutions, but the true number of independent solutions are two. Following the yellow book, we fix $s = s_+$, and the two independent solutions are written as

$$\begin{aligned}
r = r_- : f_1^{(-)} &= F\left(\frac{1}{\kappa}, -\frac{1}{\kappa}; 1 - \frac{N}{\kappa}; x\right) , \\
r = r_+ : f_1^{(+)} &= F\left(\frac{N-1}{\kappa}, \frac{N+1}{\kappa}; 1 + \frac{N}{\kappa}; x\right) .
\end{aligned} \tag{A.31}$$

Then, the two solutions of F_1 become

$$F_1^{(-)}(x) = x^{-2h}(1-x)^{h_{\hat{\theta}}-2h} F\left(\frac{1}{\kappa}, -\frac{1}{\kappa}; 1 - \frac{N}{\kappa}; x\right) , \tag{A.32}$$

$$F_1^{(+)}(x) = x^{h_{\hat{\theta}}-2h}(1-x)^{h_{\hat{\theta}}-2h} F\left(\frac{N-1}{\kappa}, \frac{N+1}{\kappa}; 1 + \frac{N}{\kappa}; x\right) . \tag{A.33}$$

By plugging these solutions to (A.25), we obtain the solutions for F_2 :¹⁹

$$F_2^{(-)}(x) = \frac{1}{k} x^{1-2h}(1-x)^{h_{\hat{\theta}}-2h} F\left(1 + \frac{1}{\kappa}, 1 - \frac{1}{\kappa}; 2 - \frac{N}{\kappa}; x\right) , \tag{A.34}$$

$$F_2^{(+)}(x) = -N x^{h_{\hat{\theta}}-2h}(1-x)^{h_{\hat{\theta}}-2h} F\left(\frac{N-1}{\kappa}, \frac{N+1}{\kappa}; \frac{N}{\kappa}; x\right) . \tag{A.35}$$

¹⁹Remark that there is a typo in [67, equation (15.170)].

These results imply that $F_A^{(-)}(A = 1, 2)$ are conformal blocks for the identity channel, while $F_A^{(+)}(A = 1, 2)$ are conformal blocks for the adjoint field channel.

By restoring the dependence on the anti-holomorphic coordinate, the four-point function can be written as

$$F_{ik}^{j\ell}(x, \bar{x}) := \langle \Phi_i(x, \bar{x}) \Phi^{\dagger j}(0, 0) \Phi^{\dagger \ell}(1, 1) \Phi_k(\infty, \infty) \rangle = \sum_{A,B=1,2} (I_A)^{j\ell}_{ik} (\bar{I}_B)^{j\ell}_{ik} G_{AB}(x, \bar{x}) , \quad (\text{A.36})$$

where $G_{A,B}$ is given by

$$G_{A,B}(x, \bar{x}) = \sum_{\alpha, \beta = \pm} X_{\alpha, \beta} F_A^{(\alpha)}(x) F_B^{(\beta)}(\bar{x}) , \quad (\text{A.37})$$

with some coefficient $X_{\alpha, \beta}$. Physical correlation functions must satisfy the locality condition and the crossing-symmetry, which can be used to fix coefficients $X_{\alpha, \beta}$. The locality condition is given by

$$G_{AB}(e^{2\pi i} x, e^{-2\pi i} \bar{x}) = G_{AB}(x, \bar{x}) . \quad (\text{A.38})$$

This clearly prohibits the off-diagonal contributions:

$$X_{-+} = X_{+-} = 0 . \quad (\text{A.39})$$

The second condition is the crossing-symmetry:

$$F_{ik}^{j\ell}(x, \bar{x}) = F_{ik}^{\ell j}(1 - x, 1 - \bar{x}) , \quad (\text{A.40})$$

which is equivalent to

$$G_{A,B}(x, \bar{x}) = G_{3-A, 3-B}(1 - x, 1 - \bar{x}) . \quad (\text{A.41})$$

This crossing symmetry can be used to fix the remaining coefficients X_{++} and X_{--} as seen below. Thanks to the following identity:

$$F(a, b; c; x) = A_1 F(a, b; a + b - c + 1; 1 - x) + A_2 (1 - x)^{c-a-b} F(c - a, c - b; c - a - b + 1; 1 - x) , \quad (\text{A.42})$$

where A_1 and A_2 are given by

$$A_1 = \frac{\Gamma(c)\Gamma(c-a-b)}{\Gamma(c-a)\Gamma(c-b)} , \quad A_2 = \frac{\Gamma(c)\Gamma(a+b-c)}{\Gamma(a)\Gamma(b)} . \quad (\text{A.43})$$

one can write down the conformal blocks as the power series of $1 - x$. This implies that we can express the conformal blocks $F_A^{(\alpha)}(x)$ as follows:²⁰

$$F_A^{(\alpha)}(x) = \sum_{\beta} c_{\alpha\beta} F_{3-A}^{(\beta)}(1 - x) . \quad (\text{A.44})$$

²⁰Recall that the crossing symmetry flips I_1 and I_2 .

Clearly, the matrix $c_{\alpha\beta}$ must satisfy the idempotent condition:

$$c_{++} = -c_{--} \ , \quad c_{++}^2 + c_{+-}c_{-+} = 1 \ . \quad (\text{A.45})$$

After some computations, one can fix c_{--} and c_{+-} as

$$c_{--} = N \frac{\Gamma(N/\kappa)\Gamma(-N/\kappa)}{\Gamma(1/\kappa)\Gamma(-1/\kappa)} \ , \quad c_{+-} = -N \frac{\Gamma(N/\kappa)^2}{\Gamma((N+1)/\kappa)\Gamma((N-1)/\kappa)} \ . \quad (\text{A.46})$$

By substituting (A.44) into (A.41), the crossing relation (A.41) is equivalent to

$$\sum_{\gamma,\delta} X_{\gamma\delta} c_{\gamma\alpha} c_{\delta\beta} = X_{\alpha\beta} \ . \quad (\text{A.47})$$

More explicitly, these can be written as

$$X_{++}c_{++}c_{+-} + X_{--}c_{-+}c_{--} = 0 \ , \quad (\text{A.48})$$

$$X_{--}c_{--}^2 + X_{++}c_{+-}^2 = X_{--} \ , \quad (\text{A.49})$$

$$X_{--}c_{-+}^2 + X_{++}c_{++}^2 = X_{++} \ , \quad (\text{A.50})$$

where we used (A.39). By using (A.45), these constraints are reduced to

$$X_{++} = \frac{1 - c_{--}^2}{c_{+-}^2} X_{--} \ . \quad (\text{A.51})$$

By choosing the normalization $X_{--} = 1$, one can obtain the physical four-point function satisfying both the locality condition and the crossing symmetry:

$$G_{AB}(x, \bar{x}) = F_A^{(-)}(x) F_B^{(-)}(\bar{x}) + \frac{1 - c_{--}^2}{c_{+-}^2} F_A^{(+)}(x) F_B^{(+)}(\bar{x}) \ . \quad (\text{A.52})$$

Note that only when $k = 1$, the second term vanishes due to $c_{--} = 1$. This means that the only identity block contributes to the four-point function. This is consistent with the fusion rule of WZW primaries.

B Asymptotic behavior of EA_2 in $\widehat{su}(N)_k$ WZW model

In this appendix, we derive the asymptotic behavior of EA_2 in $\widehat{su}(N)_k$ WZW model. For later convenience, let us consider the case in which the following parameters ϵ_{\pm} are infinitesimally small:

$$\epsilon_{\pm} = \frac{1}{4} \left(\frac{\tilde{\tau}_0}{(\tilde{t} \pm \tilde{x}_0)(\tilde{t} \pm \tilde{x}_0 \mp 1) + \tilde{\tau}_0^2} \right)^2 \ , \quad (\text{B.1})$$

where $\tilde{\tau}_0 = \frac{\tau_0}{\ell}$, $\tilde{x}_0 = \frac{x_0}{\ell}$ and $\tilde{t} = \frac{t}{\ell}$ are dimensionless parameters. In this case, the cross-ratios x in (2.34) and \bar{x} in (2.35) can be approximated as

$$x = \begin{cases} 1 - \epsilon_+ & , \quad (\tilde{t} + \tilde{x}_0) (\tilde{t} + \tilde{x}_0 - 1) + \tilde{\tau}_0^2 \geq 0 \\ \epsilon_+ & , \quad (\tilde{t} + \tilde{x}_0) (\tilde{t} + \tilde{x}_0 - 1) + \tilde{\tau}_0^2 < 0 \end{cases} \quad (\text{B.2})$$

$$\bar{x} = \begin{cases} 1 - \epsilon_- & , \quad (\tilde{t} - \tilde{x}_0) (\tilde{t} - \tilde{x}_0 + 1) + \tilde{\tau}_0^2 \geq 0 \\ \epsilon_- & , \quad (\tilde{t} - \tilde{x}_0) (\tilde{t} - \tilde{x}_0 + 1) + \tilde{\tau}_0^2 < 0 \end{cases}$$

Since EA_2 essentially depends on x , \bar{x} , N and k , we denote it as $\Delta S_A^{(2)}(x, \bar{x}; N, k)$. Note that this notation differs from that used in the main text. In the following, we derive the asymptotic behaviors of EA_2 in various limits.

Long time limit: $\tilde{t} \rightarrow \infty$.

For $\tilde{t} \gg \tilde{\tau}_0$, the infinitesimally small parameter ϵ_{\pm} take the form:

$$\epsilon_{\pm} = \epsilon = \frac{1}{4} \left(\frac{\tilde{\tau}_0}{\tilde{t}^2} \right)^2, \quad (\text{B.3})$$

and the cross-ratios in (B.2) are given by

$$(x, \bar{x}) = (1 - \epsilon, 1 - \epsilon). \quad (\text{B.4})$$

In the limit $(x, \bar{x}) \rightarrow (1, 1)$, the 4pt function $G_{2,2}$ dominates in (3.9), and EA_2 converges to zero. The asymptotic behavior is obtained by expanding EA_2 with respect to ϵ :

$$\Delta S_A^{(2)}(1 - \epsilon, 1 - \epsilon; N, k) = \frac{(N-1)(N^2-2)}{N^2(N+1)} c_{N,k} \epsilon^{\frac{2N}{N+k}} + \frac{2}{k} \left(1 - \frac{1}{N} \right) \epsilon + \mathcal{O} \left(\epsilon^{1+\frac{2N}{N+k}} \right) \quad (\text{B.5})$$

where the coefficient $c_{N,k}$ is given by

$$c_{N,k} = \frac{\Gamma \left(\frac{k}{N+k} \right)^2 \Gamma \left(\frac{N-1}{N+k} \right) \Gamma \left(\frac{N+1}{N+k} \right)}{\Gamma \left(\frac{N}{N+k} \right)^2 \Gamma \left(\frac{k-1}{N+k} \right) \Gamma \left(\frac{k+1}{N+k} \right)} \geq 0. \quad (\text{B.6})$$

Note that EA_2 is positive and decays to zero as $\epsilon \rightarrow 0$. In this expansion, the first term $\mathcal{O}(\epsilon^{2N/(N+k)})$ dominates for $N < k$, while the second term $\mathcal{O}(\epsilon)$ dominates for $k < N$.

For $N = k$, the coefficient reduces to $c_{N,N} = 1$, and the two contributions merge into:

$$\Delta S_A^{(2)}(1 - \epsilon, 1 - \epsilon; N, N) = \left(1 - \frac{2}{N(N+1)} \right) \epsilon + \mathcal{O}(\epsilon^2). \quad (\text{B.7})$$

A same analysis applies to other limits, such as $\tilde{\tau}_0 \rightarrow \infty$ and $\tilde{x}_0 \rightarrow 0$. In those cases, the infinitesimal parameter ϵ is replaced by

$$\epsilon = \frac{1}{4} \left(\frac{1}{\tilde{\tau}_0} \right)^2, \quad \tilde{\tau}_0 \rightarrow \infty$$

$$\epsilon = \frac{1}{4} \left(\frac{\tilde{\tau}_0}{\tilde{x}_0^2} \right)^2, \quad |\tilde{x}_0| \rightarrow \infty. \quad (\text{B.8})$$

Large interval limit: $\tilde{\tau}_0 \rightarrow 0$.

Let us now consider the case $\tilde{\tau}_0 \ll |\tilde{t} \pm \tilde{x}_0|$. For $\tilde{x}_0 < 0$, the time dependence of the cross-ratios (B.2) is given by

$$\lim_{\tilde{\tau}_0 \rightarrow 0} (x(t), \bar{x}(t)) = \begin{cases} (1, 1) & , 0 \leq \tilde{t} \leq |\tilde{x}_0|, |\tilde{x}_0| + 1 \leq \tilde{t} \\ (0, 1) & , |\tilde{x}_0| < \tilde{t} < |\tilde{x}_0| + 1 \end{cases} , \quad (\text{B.9})$$

where we have neglected the $\mathcal{O}(\epsilon_{\pm})$ terms for simplicity. When $(x, \bar{x}) \rightarrow (1, 1)$, the contribution from G_{22} dominates over the other terms G_{11} , G_{12} and G_{21} , due to the explicit form of $F_A^{\pm}(x)$ in (A.32)-(A.35) together with the crossing symmetry (A.41). As a result, EA_2 in (3.9) converges to zero. In contrast, when $(x, \bar{x}) \rightarrow (0, 1)$, G_{12} dominates over G_{11} , G_{21} and G_{22} , owing to the relation (A.44), and EA_2 converges to $\log N$. We may summarize this behavior as

$$\lim_{\tilde{\tau}_0 \rightarrow 0} \Delta S_A^{(2)} = \begin{cases} 0 & , 0 \leq \tilde{t} \leq |\tilde{x}_0|, |\tilde{x}_0| + 1 \leq \tilde{t} \\ \log N & , |\tilde{x}_0| < \tilde{t} < |\tilde{x}_0| + 1 \end{cases} , \quad (\text{B.10})$$

A qualitatively similar behavior holds for $1 < \tilde{x}_0$.

For $0 < \tilde{x}_0 < 1$, the time dependence of the cross-ratios (B.2) changes as

$$\lim_{\tilde{\tau}_0 \rightarrow 0} (x(t), \bar{x}(t)) = \begin{cases} (0, 0) & , 0 \leq \tilde{t} \leq \tilde{x}_0 \\ (0, 1) & , \tilde{x}_0 < \tilde{t} < 1 - \tilde{x}_0 \\ (1, 1) & , 1 - \tilde{x}_0 \leq \tilde{t} \end{cases} , \quad (\text{B.11})$$

where we have assumed $0 < \tilde{x}_0 < 1/2$ (a similar argument applies to for $1/2 < \tilde{x}_0 < 1$). In this regime, when $(x, \bar{x}) \rightarrow (0, 0)$, the G_{11} dominates over G_{12} , G_{21} and G_{22} , and EA_2 converges to $\log[N(N+1)/2]$. Thus, the time evolution of EA_2 can be summarized as

$$\lim_{\tilde{\tau}_0 \rightarrow 0} \Delta S_A^{(2)} = \begin{cases} \log \left[\frac{N(N+1)}{2} \right] & , 0 \leq \tilde{t} \leq \tilde{x}_0 \\ \log N & , \tilde{x}_0 < \tilde{t} < 1 - \tilde{x}_0 \\ 0 & , 1 - \tilde{x}_0 \leq \tilde{t} \end{cases} , \quad (\text{B.12})$$

Here, we have omitted the infinitesimally small corrections of order $\mathcal{O}(\epsilon_{\pm})$. In the following, we derive the explicit form of those terms in the special cases relevant to the quantum Mpemba effect.

- Case 1: $\tilde{\tau}_0 \rightarrow 0$, $\tilde{t} = 0$, $0 < \tilde{x}_0 < 1$

This corresponds to the left panel of Fig. 6 in the limit $\tilde{\tau}_0 \rightarrow 0$. The cross-ratios take the form

$$(x, \bar{x}) = (\epsilon, \epsilon) , \quad (\text{B.13})$$

where the infinitesimally small parameter ϵ is given by

$$\epsilon = \frac{1}{4} \left(\frac{\tilde{\tau}_0}{\tilde{x}_0(\tilde{x}_0 - 1)} \right)^2. \quad (\text{B.14})$$

Expanding EA_2 with respect to ϵ , we obtain the next leading correction:

$$\Delta S_A^{(2)} = \log \left[\frac{N(N+1)}{2} \right] - \frac{(N-1)(N^2+2N-2)}{2N} c_{N,k} \epsilon^{\frac{2N}{N+k}} - \frac{N-1}{k} \epsilon + \mathcal{O} \left(\epsilon^{1+\frac{2N}{N+k}} \right). \quad (\text{B.15})$$

In this expansion, the first term $\mathcal{O}(\epsilon^{2N/(N+k)})$ dominates for $N < k$, while the second term $\mathcal{O}(\epsilon)$ dominates for $k < N$. For $N = k$, the two terms merge and EA_2 becomes

$$\Delta S_A^{(2)} = \log \left[\frac{N(N+1)}{2} \right] - \frac{1}{2} (N-1)(N+2) \epsilon + \mathcal{O}(\epsilon^2). \quad (\text{B.16})$$

- Case 2: $\tilde{\tau}_0 \ll \tilde{\delta}$, $\tilde{t} = +\tilde{\delta}$, $\tilde{x}_0 = 0$

This corresponds to the right panel of Fig. 6 in the limit $\tilde{\tau}_0 \rightarrow 0$. The cross-ratios take the form

$$(x, \bar{x}) = (\epsilon, 1 - \epsilon), \quad (\text{B.17})$$

where the infinitesimally small parameter ϵ is given by

$$\epsilon = \frac{1}{4} \left(\frac{\tilde{\tau}_0}{\tilde{\delta}} \right)^2. \quad (\text{B.18})$$

Expanding EA_2 with respect to ϵ , we obtain the next leading correction:

$$\Delta S_A^{(2)} = \log N - d_{N,k} \epsilon^{\frac{N}{N+k}} - \left(N - 2 + \frac{2}{N+1} \right) \epsilon + \mathcal{O} \left(\epsilon^{1+\frac{N}{N+k}} \right) \quad (\text{B.19})$$

with the coefficient $d_{N,k}$ defined by

$$d_{N,k} = \frac{N(N-1)}{N+1} \frac{\Gamma\left(\frac{1}{N+k}\right) \Gamma\left(1 - \frac{1}{N+k}\right) \Gamma\left(\frac{k}{N+k}\right)}{\Gamma\left(\frac{k-1}{N+k}\right) \Gamma\left(\frac{k+1}{N+k}\right) \Gamma\left(\frac{N}{N+k}\right)}. \quad (\text{B.20})$$

Note that $d_{N,k}$ is positive for $k \geq 2$ and vanishes for $k = 1$. Consequently, the next leading contribution is the second term $\mathcal{O}(\epsilon^{\frac{N}{N+k}})$ for $k \geq 2$, while for $k = 1$ it is the $\mathcal{O}(\epsilon)$ term.

References

- [1] F. Ares, S. Murciano, and P. Calabrese, “Entanglement asymmetry as a probe of symmetry breaking,” *Nature Commun.* **14** no. 1, (2023) 2036, [arXiv:2207.14693](#) [[cond-mat.stat-mech](#)].

- [2] S. Kullback and R. A. Leibler, “On Information and Sufficiency,” *The Annals of Mathematical Statistics* **22** no. 1, (1951) 79–86.
- [3] M. Chen and H.-H. Chen, “Rényi entanglement asymmetry in (1+1)-dimensional conformal field theories,” *Phys. Rev. D* **109** no. 6, (2024) 065009, [arXiv:2310.15480 \[hep-th\]](#).
- [4] M. Fossati, F. Ares, J. Dubail, and P. Calabrese, “Entanglement asymmetry in CFT and its relation to non-topological defects,” *JHEP* **05** (2024) 059, [arXiv:2402.03446 \[hep-th\]](#).
- [5] L. Capizzi and M. Mazzoni, “Entanglement asymmetry in the ordered phase of many-body systems: the Ising field theory,” *JHEP* **2023** no. 12, (2023) 144, [arXiv:2307.12127 \[cond-mat.stat-mech\]](#).
- [6] M. Lastres, S. Murciano, F. Ares, and P. Calabrese, “Entanglement asymmetry in the critical XXZ spin chain,” *J. Stat. Mech.* **2025** no. 1, (2025) 013107, [arXiv:2407.06427 \[cond-mat.stat-mech\]](#).
- [7] M. Fossati, C. Rylands, and P. Calabrese, “Entanglement asymmetry in CFT with boundary symmetry breaking,” *JHEP* **06** (2025) 089, [arXiv:2411.10244 \[hep-th\]](#).
- [8] Y. Kusuki, S. Murciano, H. Ooguri, and S. Pal, “Entanglement asymmetry and symmetry defects in boundary conformal field theory,” *JHEP* **01** (2025) 057, [arXiv:2411.09792 \[hep-th\]](#).
- [9] L. K. Joshi *et al.*, “Observing the Quantum Mpemba Effect in Quantum Simulations,” *Phys. Rev. Lett.* **133** no. 1, (2024) 010402, [arXiv:2401.04270 \[quant-ph\]](#).
- [10] J. Zhang, G. Xia, C.-W. Wu, T. Chen, Q. Zhang, Y. Xie, W.-B. Su, W. Wu, C.-W. Qiu, P.-X. Chen, W. Li, H. Jing, and Y.-L. Zhou, “Observation of quantum strong mpemba effect,” *Nature Communications* **16** no. 1, (Jan., 2025) . <http://dx.doi.org/10.1038/s41467-024-54303-0>.
- [11] S. Aharony Shapira, Y. Shapira, J. Markov, G. Teza, N. Akerman, O. Raz, and R. Ozeri, “Inverse Mpemba Effect Demonstrated on a Single Trapped Ion Qubit,” *Phys. Rev. Lett.* **133** no. 1, (2024) 010403, [arXiv:2401.05830 \[quant-ph\]](#).
- [12] Y. Xu *et al.*, “Observation and Modulation of the Quantum Mpemba Effect on a Superconducting Quantum Processor,” [arXiv:2508.07707 \[quant-ph\]](#).
- [13] F. Ares, S. Murciano, E. Vernier, and P. Calabrese, “Lack of symmetry restoration after a quantum quench: An entanglement asymmetry study,” *SciPost Phys.* **15** no. 3, (2023) 089, [arXiv:2302.03330 \[cond-mat.stat-mech\]](#).

- [14] F. Ares, V. Vitale, and S. Murciano, “Quantum Mpemba effect in free-fermionic mixed states,” *Phys. Rev. B* **111** no. 10, (2025) 104312, [arXiv:2405.08913 \[cond-mat.stat-mech\]](#).
- [15] F. Ferro, F. Ares, and P. Calabrese, “Non-equilibrium entanglement asymmetry for discrete groups: the example of the XY spin chain,” *J. Stat. Mech.* **2402** (2024) 023101, [arXiv:2307.06902 \[cond-mat.stat-mech\]](#).
- [16] C. Rylands, E. Vernier, and P. Calabrese, “Dynamical symmetry restoration in the Heisenberg spin chain,” *J. Stat. Mech.* **2024** no. 12, (2024) 123102, [arXiv:2409.08735 \[cond-mat.stat-mech\]](#).
- [17] K. Chalas, F. Ares, C. Rylands, and P. Calabrese, “Multiple crossings during dynamical symmetry restoration and implications for the quantum Mpemba effect,” *J. Stat. Mech.* **2024** no. 10, (2024) 103101, [arXiv:2405.04436 \[cond-mat.stat-mech\]](#).
- [18] S. Liu, H.-K. Zhang, S. Yin, S.-X. Zhang, and H. Yao, “Quantum Mpemba effects in many-body localization systems,” [arXiv:2408.07750 \[cond-mat.dis-nn\]](#).
- [19] T. Bhore, L. Su, I. Martin, A. A. Clerk, and Z. Papić, “Quantum Mpemba effect without global symmetries,” [arXiv:2505.17181 \[quant-ph\]](#).
- [20] F. Ares, C. Rylands, and P. Calabrese, “A simpler probe of the quantum Mpemba effect in closed systems,” [arXiv:2507.05946 \[cond-mat.stat-mech\]](#).
- [21] S. Yamashika and F. Ares, “The quantum Mpemba effect in long-range spin systems,” [arXiv:2507.06636 \[cond-mat.stat-mech\]](#).
- [22] M. Gibbins, A. Smith, and B. Bertini, “Translation symmetry restoration in integrable systems: the noninteracting case,” [arXiv:2506.14555 \[cond-mat.stat-mech\]](#).
- [23] S. Yamashika, F. Ares, and P. Calabrese, “Entanglement asymmetry and quantum Mpemba effect in two-dimensional free-fermion systems,” *Phys. Rev. B* **110** no. 8, (2024) 085126, [arXiv:2403.04486 \[cond-mat.stat-mech\]](#).
- [24] S. Yamashika, P. Calabrese, and F. Ares, “Quenching from superfluid to free bosons in two dimensions: Entanglement, symmetries, and the quantum Mpemba effect,” *Phys. Rev. A* **111** no. 4, (2025) 043304, [arXiv:2410.14299 \[cond-mat.stat-mech\]](#).
- [25] F. Benini, V. Godet, and A. H. Singh, “Entanglement asymmetry in conformal field theory and holography,” [arXiv:2407.07969 \[hep-th\]](#).
- [26] S. Liu, H.-K. Zhang, S. Yin, and S.-X. Zhang, “Symmetry Restoration and Quantum Mpemba Effect in Symmetric Random Circuits,” *Phys. Rev. Lett.* **133** no. 14, (2024) 140405, [arXiv:2403.08459 \[quant-ph\]](#).

- [27] X. Turkeshi, P. Calabrese, and A. De Luca, “Quantum Mpemba Effect in Random Circuits,” *Phys. Rev. Lett.* **135** no. 4, (2025) 040403, [arXiv:2405.14514 \[quant-ph\]](#).
- [28] F. Ares, S. Murciano, P. Calabrese, and L. Piroli, “Entanglement asymmetry dynamics in random quantum circuits,” [arXiv:2501.12459 \[cond-mat.stat-mech\]](#).
- [29] H. Yu, Z.-X. Li, and S.-X. Zhang, “Symmetry Breaking Dynamics in Quantum Many-Body Systems,” [arXiv:2501.13459 \[quant-ph\]](#).
- [30] K. Klobas, C. Rylands, and B. Bertini, “Translation symmetry restoration under random unitary dynamics,” *Phys. Rev. B* **111** no. 14, (2025) L140304, [arXiv:2406.04296 \[cond-mat.stat-mech\]](#).
- [31] A. Russotto, F. Ares, and P. Calabrese, “Non-Abelian entanglement asymmetry in random states,” *JHEP* **06** (2025) 149, [arXiv:2411.13337 \[hep-th\]](#).
- [32] H.-H. Chen and Z.-J. Tang, “Entanglement asymmetry in the Hayden-Preskill protocol,” *Phys. Rev. D* **111** no. 6, (2025) 066003, [arXiv:2411.17695 \[hep-th\]](#).
- [33] T. Banerjee, S. Das, and K. Sengupta, “Entanglement asymmetry in periodically driven quantum systems,” [arXiv:2412.03654 \[quant-ph\]](#).
- [34] K. Klobas, “Non-equilibrium dynamics of symmetry-resolved entanglement and entanglement asymmetry: exact asymptotics in Rule 54*,” *J. Phys. A* **57** no. 50, (2024) 505001, [arXiv:2407.21793 \[cond-mat.stat-mech\]](#).
- [35] F. Ares, P. Calabrese, and S. Murciano, “The quantum Mpemba effects,” [arXiv:2502.08087 \[cond-mat.stat-mech\]](#).
- [36] H. Yu, S. Liu, and S.-X. Zhang, “Quantum Mpemba effects from symmetry perspectives,” *AAPPS Bull.* **35** no. 1, (2025) 17, [arXiv:2507.02301 \[quant-ph\]](#).
- [37] L. Capizzi and V. Vitale, “A universal formula for the entanglement asymmetry of matrix product states,” *J. Phys. A* **57** no. 45, (2024) 45LT01, [arXiv:2310.01962 \[quant-ph\]](#).
- [38] N. D. Mermin and H. Wagner, “Absence of ferromagnetism or antiferromagnetism in one-dimensional or two-dimensional isotropic Heisenberg models,” *Phys. Rev. Lett.* **17** (1966) 1133–1136.
- [39] S. R. Coleman, “There are no Goldstone bosons in two-dimensions,” *Commun. Math. Phys.* **31** (1973) 259–264.
- [40] M. Nozaki, T. Numasawa, and T. Takayanagi, “Quantum Entanglement of Local Operators in Conformal Field Theories,” *Phys. Rev. Lett.* **112** (2014) 111602, [arXiv:1401.0539 \[hep-th\]](#).

- [41] V. G. Knizhnik and A. B. Zamolodchikov, “Current Algebra and Wess-Zumino Model in Two-Dimensions,” *Nucl. Phys. B* **247** (1984) 83–103.
- [42] P. Christe and R. Flume, “The Four Point Correlations of All Primary Operators of the $d = 2$ Conformally Invariant $SU(2)$ σ Model With Wess-Zumino Term,” *Nucl. Phys. B* **282** (1987) 466.
- [43] A. B. Zamolodchikov and V. A. Fateev, “Operator Algebra and Correlation Functions in the Two-Dimensional Wess-Zumino $SU(2) \times SU(2)$ Chiral Model,” *Sov. J. Nucl. Phys.* **43** (1986) 657–664.
- [44] C. Holzhey, F. Larsen, and F. Wilczek, “Geometric and renormalized entropy in conformal field theory,” *Nucl. Phys. B* **424** (1994) 443–467, [arXiv:hep-th/9403108](#).
- [45] P. Calabrese and J. L. Cardy, “Entanglement entropy and quantum field theory,” *J. Stat. Mech.* **0406** (2004) P06002, [arXiv:hep-th/0405152](#).
- [46] H. Casini and M. Huerta, “Entanglement entropy in free quantum field theory,” *J. Phys. A* **42** (2009) 504007, [arXiv:0905.2562 \[hep-th\]](#).
- [47] D. Gaiotto, A. Kapustin, N. Seiberg, and B. Willett, “Generalized Global Symmetries,” *JHEP* **02** (2015) 172, [arXiv:1412.5148 \[hep-th\]](#).
- [48] L. Bhardwaj, L. E. Bottini, L. Fraser-Taliente, L. Gladden, D. S. W. Gould, A. Platschorre, and H. Tillim, “Lectures on generalized symmetries,” *Phys. Rept.* **1051** (2024) 1–87, [arXiv:2307.07547 \[hep-th\]](#).
- [49] M. A. Nielsen and I. L. Chuang, *Quantum Computation and Quantum Information*. Cambridge University Press, 6, 2012.
- [50] M. Goldstein and E. Sela, “Symmetry-resolved entanglement in many-body systems,” *Phys. Rev. Lett.* **120** no. 20, (2018) 200602, [arXiv:1711.09418 \[cond-mat.stat-mech\]](#).
- [51] E. Cornfeld, M. Goldstein, and E. Sela, “Imbalance entanglement: Symmetry decomposition of negativity,” *Phys. Rev. A* **98** no. 3, (2018) 032302, [arXiv:1804.00632 \[cond-mat.stat-mech\]](#).
- [52] S. He, T. Numasawa, T. Takayanagi, and K. Watanabe, “Quantum dimension as entanglement entropy in two dimensional conformal field theories,” *Phys. Rev. D* **90** no. 4, (2014) 041701, [arXiv:1403.0702 \[hep-th\]](#).
- [53] K. Ohmori and Y. Tachikawa, “Physics at the entangling surface,” *J. Stat. Mech.* **1504** (2015) P04010, [arXiv:1406.4167 \[hep-th\]](#).

- [54] W.-Z. Guo and S. He, “Rényi entropy of locally excited states with thermal and boundary effect in 2D CFTs,” *JHEP* **04** (2015) 099, [arXiv:1501.00757 \[hep-th\]](#).
- [55] M. Creutz, “ON INVARIANT INTEGRATION OVER $SU(N)$,” *J. Math. Phys.* **19** (1978) 2043.
- [56] P. Calabrese and J. L. Cardy, “Evolution of entanglement entropy in one-dimensional systems,” *J. Stat. Mech.* **0504** (2005) P04010, [arXiv:cond-mat/0503393](#).
- [57] V. Alba and P. Calabrese, “Entanglement and thermodynamics after a quantum quench in integrable systems,” *Proc. Nat. Acad. Sci.* **114** no. 30, (2017) 7947.
- [58] S. V. Ketov, *Conformal field theory*. 1995.
- [59] B. Collins and S. Matsumoto, “On some properties of orthogonal weingarten functions,” *Journal of Mathematical Physics* **50** no. 11, (Nov., 2009) .
<http://dx.doi.org/10.1063/1.3251304>.
- [60] D. Weingarten, “Asymptotic Behavior of Group Integrals in the Limit of Infinite Rank,” *J. Math. Phys.* **19** (1978) 999.
- [61] J. Fuchs, “Superconformal Ward Identities and the WZW Model,” *Nucl. Phys. B* **286** (1987) 455–484.
- [62] J. Fuchs, “Free Fermions and WZW Theories on Nonsimple Groups,” *Z. Phys. C* **35** (1987) 89.
- [63] J. Cardy and C. P. Herzog, “Universal Thermal Corrections to Single Interval Entanglement Entropy for Two Dimensional Conformal Field Theories,” *Phys. Rev. Lett.* **112** no. 17, (2014) 171603, [arXiv:1403.0578 \[hep-th\]](#).
- [64] M. Ghasemi, “Universal thermal corrections to symmetry-resolved entanglement entropy and full counting statistics,” *JHEP* **05** (2023) 209, [arXiv:2203.06708 \[hep-th\]](#).
- [65] B. Chen and J.-q. Wu, “Single interval Renyi entropy at low temperature,” *JHEP* **08** (2014) 032, [arXiv:1405.6254 \[hep-th\]](#).
- [66] E. Witten, “Quantum Field Theory and the Jones Polynomial,” *Commun. Math. Phys.* **121** (1989) 351–399.
- [67] P. Di Francesco, P. Mathieu, and D. Senechal, *Conformal Field Theory*. Graduate Texts in Contemporary Physics. Springer-Verlag, New York, 1997.